PSI-1085/TR-1237

# ENERGY TRANSFER STUDIES IN INTERHALOGEN MOLECULES



Prepared by:

S.J. Davis
K.W. Holtzclaw
W.J. Kessler
L.G. Piper

Physical Sciences Inc.
20 New England Business Center
Andover, MA 01810

Final Report

January 1993

Contract No. F49620-89-C-0101



Prepared for:

USAF, AFSC
Air Force Office of Scientific Research
Building 410
Bolling AFB, DC 20332-6448

# REPORT DOCUMENTATION PAGE

Form Approved
OMB No. 0704-0188



| 1. AGENCY USE ONLY (Leave blank) | 2. REPORT DATE | 3. REPORT TYPE AND DATES COVERED |
|---|---|---|
| | January 1993 | Final |

**4. TITLE AND SUBTITLE**

Energy Transfer Studies in Interhalogen Molecules

**5. FUNDING NUMBERS**

C
F49620-89-C-0101

**6. AUTHOR(S)**

S.J. Davis, K.W. Holtzclaw, W.J. Kessler, L.G. Piper

**7. PERFORMING ORGANIZATION NAME(S) AND ADDRESS(ES)**

Physical Sciences Inc.
20 New England Business Center
Andover, MA 01810

**8. PERFORMING ORGANIZATION REPORT NUMBER**

PSI-1085/TR-1237

**9. SPONSORING/MONITORING AGENCY NAME(S) AND ADDRESS(ES)**

USAF, AFMC
Air Force of Scientific Research
Bldg. 410
Bolling AFB, DC 20332-6448

**10. SPONSORING/MONITORING AGENCY REPORT NUMBER**

**11. SUPPLEMENTARY NOTES**

**12a. DISTRIBUTION/AVAILABILITY STATEMENT**

Approved for public release;
distribution unlimited.

**12b. DISTRIBUTION CODE**

**13. ABSTRACT (Maximum 200 words)**

This program is examining energy transfer processes in interhalogen molecules that have potential for visible chemical laser development. Spectrally resolved laser induced fluorescence is used to determine rotation-to-translation (R-T) and vibration-to-translation (V-T) rate coefficients. In this report we compare several fitting laws for R-T transfer to data obtained for IF and IC1 interactions with several collision partners. We have also obtained preliminary data on V-T relaxation within the ground electronic state of IF. Preliminary results of an optically-pumped HF laser are also presented.

**14. SUBJECT TERMS**

Energy transfer, Laser excitation, Laser induced fluorescence, Amplified spontaneous emission

**15. NUMBER OF PAGES**

**16. PRICE CODE**

| 17. SECURITY CLASSIFICATION OF REPORT | 18. SECURITY CLASSIFICATION OF THIS PAGE | 19. SECURITY CLASSIFICATION OF ABSTRACT | 20. LIMITATION OF ABSTRACT |
|---|---|---|---|
| Unclassified | Unclassified | Unclassified | |

CLASSIFIED BY

DECLASSIFY ON

# FINAL PROJECT SUMMARY

1. TITLE: Energy Transfer in Interhalogen Molecules

2. PRINCIPAL INVESTIGATOR: Dr. Steven J. Davis

3. INCLUSIVE DATES: 15 August 1989 - 15 November 1992

4. CONTRACT/GRANT NUMBER: F49620-89-C-0101

5. COSTS AND FY SOURCE: FY89-92 $284,633

6. SENIOR RESEARCH PERSONNEL: Dr. Steven J. Davis (Principal Investigator)

7. JUNIOR RESEARCH PERSONNEL: Dr. Karl Holtzclaw, Mr. William Kessler, and Dr. L.G. Piper

8. PUBLICATIONS/PRESENTATIONS:


1. "Rotational Energy Transfer in Excited States of Halogen Molecules. I. Transfer from v'=6, J'=72 in IF $B^3\Pi$". S. J. Davis and K. W. Holtzclaw, J. Chem. Phys. 92, 1611 (1990)

2. "Collisional Dynamics of the BrCl $B^3\Pi$ State. I. Electronic Quenching." G. P. Perram and S. J. Davis, J. Chem. Phys. 93, 1720 (1990)

3. "Excitation of IF(B) by Metastable $O_2$. I. Studies Involving IF(X,v)." S. J. Davis and A. M. Woodward, J. Phys. Chem. 95, 4610 (1991).

4. "Collisional Dynamics of the BrCl $B^3\Pi$ State. II. Vibrational and Rotational Energy Transfer". G. P. Perram and S. J. Davis, J. Chem Phys 98, 373 (1993)

5. "Amplified Spontaneous Emission in $I_2$, New Observations", J. W. Glessner and S. J. Davis, J. Appl. Phys. 73, (In Press)

6. "Rotational Energy Transfer in ICl(B). Comparisons to Scaling Law Predictions". S. J. Davis and K. W. Holtzclaw, (Submitted to J. Chem. Phys.)

7. "Enhancement of Electronic Energy Transfer in IF". S. J. Davis and W. J. Kessler, Chem. Phys. Lett. (In preparation).

8. "Studies of a Dye Laser-Pumped Atomic Iodine Laser". S.J. Davis and L. Hanko, Proceedings of "Lasers 92", Houston, TX (1993, in press).

9. "Optically-pumped HF Laser Based on Overtone Pumping". S.J. Davis, W.J. Kessler, G. Hager, and H. Miller, Proceedings of "Lasers 92", Houston, TX (1993, in press).

10. "Engergy Transfer Processes in Diatomic Halogens", S.J. Davis, K.W. Holtzclaw, and W.J. Kessler, Proceedings of "Lasers 92", Houston, TX (1993, in press).

## 9. ABSTRACT OF OBJECTIVES AND ACCOMPLISHMENTS:

### A. Objectives

The objective of this project is to study energy transfer processes in selected halogen molecules. In particular, we are examining rotational to translational (R-T) and vibrational to translational (V-T) transfer in the $B(^3\Pi)$ states of IF, ICl, and $I_2$. We also examine R-T transfer during inelastic vibrational collisions. The experiments are conducted using a single frequency CW dye laser as the excitation source. With this laser, molecules can be prepared in a pure quantum state (v',J'). The resulting B→X fluorescence is spectrally resolved, and the rate coefficients for energy transfer are determined using a steady state kinetic analysis. In brief, the ratio of the fluorescence intensity from a satellite collisionally populated level ($J_f$) to that of a parent laser excited level ($J_i$) is directly proportional to the R-T rate, $k_{(i-f)}$. Knowledge of the radiative lifetime of the level $J_i$ is required in the analysis. The lifetimes of the states being investigated have been previously determined.

The R-T rate coefficients are desired for two reasons. First, they are used to test parent theoretical scaling laws that predict the dependences of $k_{(i-f)}$ upon $J_i$ and upon the change in J ($\Delta J$) during a collision. These are of importance because the scaling laws depend upon the intermolecular potentials. Thus, fundamental insight is gained from these measurements. Secondly, these measurements have great practical relevance. Many of the species being investigated are excellent candidates for electronic transition chemical lasers. The degrees of R-T relaxation in the excited state will in large measure determine the efficiency of the laser. In addition, knowledge of the R-T rates in the excited B state is useful for estimating R-T relaxation in the ground state.

We have also been examining vibrational and rotational energy transfer within the ground electronic state of IF. Relaxation processes within the ground state are crucial to the efficiency and ultimate scaling of an electronic transition laser. In this report we describe preliminary results for V-T relaxation for high vibrational levels within IF(X).

We also performed some optically pumped laser studies in the molecules $I_2$ and ICl. This provided a testbed for some of the RET and V-T relaxation studies. In addition these optically-pumped lasers can yield some valuable information concerning the spectroscopy and radiative dynamics of the excited states of the laser species.

During the contract there appeared in the literature reports concerning optical gain in the $O_4^*$ complex. The dimole is observed in chemical singlet delta generators that are used in the chemical oxygen iodine laser. We performed some spectral modelling studies in an attempt to discern possible emitters in this system. We focused on the B-X system in molecular chlorine and were able to reproduce some of the features that had been reported.

In the final year of this effort we have been examining the feasibility of developing mid-IR lasers based upon optically pumped gas phase media. These lasers would fill an important Air Force mission in asset defense. We describe several experiments that have been performed near the end of this contract.

B. Progress (Final)

We completed the following activities during this effort:

- Extensive data collection for collisions of ICl and molecular collision partners.
- Detailed analysis of RET data sets for both ICl and IF.
- Comparisons of fitting and scaling laws for RET transfer
- Preliminary rate coefficients for V-T relaxation within the ground electronic state of IF.
- Optically-pumped laser studies on the B-X systems of $I_2$ and ICl.
- Spectral modeling in support of reports in the literature concerning the possibility visible laser action in oxygen dimole emission.
- Demonstration of amplified spontaneous emission in HF following excitation of overtone bands.

We describe each of these items below.

B.1 Data collection for ICl collisional processes.

In the previous reporting period we had obtained some preliminary RET data for ICl. During the present period we extended these measurements considerably. The apparatus for these measurements is shown in Figure 1. The ring dye laser is used to prepare ICl molecules in a single rovibrational level within the electronically excited B state. We use a high resolution spectrophotometer to resolve the laser-induced fluorescence that results from the laser excitation. A 1.26m Spex monochromator with an intensified 1024-element diode array comprised the spectrophotometer. This device provides spectral resolutions on the order of 0.06 nm which is sufficient to resolve many rotational lines. Accurate and reproducible placement of the diode array at the focal plane of the high-resolution monochromator is crucial for the operation of the instrument.

The dye laser (Coherent Model 699-05) was not actively stabilized, but its stability was sufficient for the experiments performed. The linewidth of the dye laser was measured with a large frame scanning Fabry-Perot interferometer (Burleigh Model 140). The measured linewidth was less than 70 MHz which is much less than the room temperature Doppler

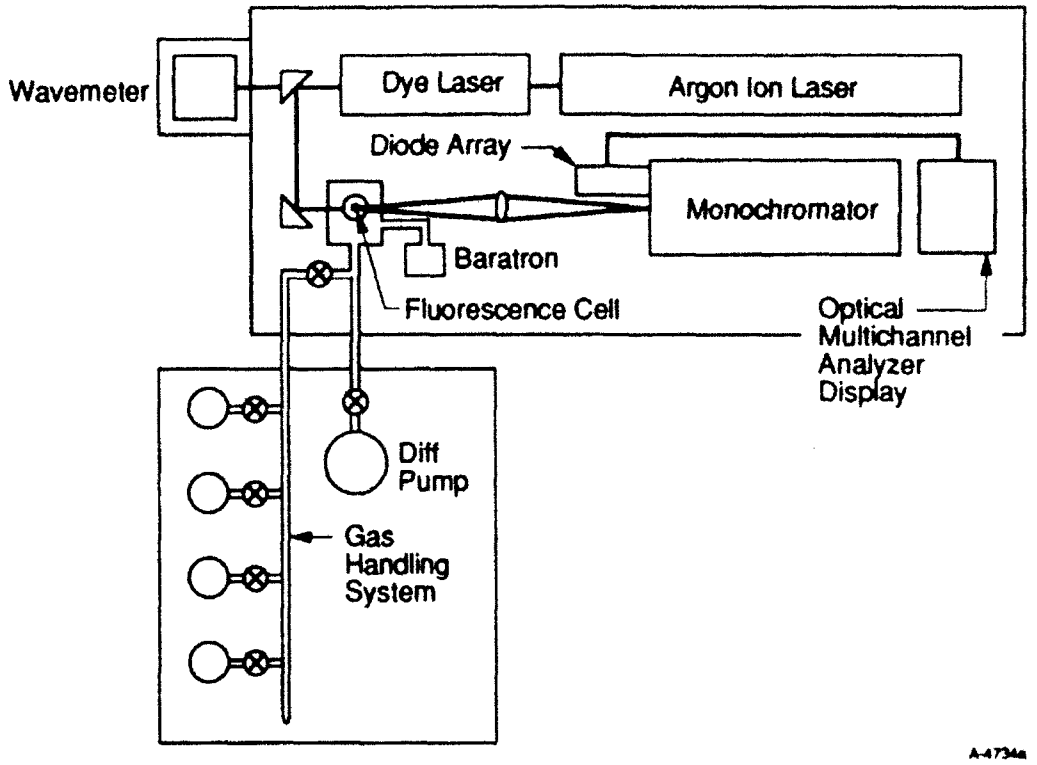


Figure 1
Block Diagram for the Apparatus used in the Rotational Energy Transfer Measurements

width (600 MHz) for the ICl absorption lines. Wavelength determination of the dye laser was accomplished using a Burleigh Model WN-20 wavemeter. The spectral purity, i.e., longitudinal mode behavior was continuously monitored using a Tropel Model 240 confocal spectrum analyzer.

ICl was produced off-line in a pyrex flask that contained $ICl_3$ crystals. The vapor above this solid is predominately ICl and $Cl_2$. The $Cl_2$ reactively removes any $I_2$ vapor. This is an important advantage since the strong and spectrally dense iodine B-X absorption system overlaps and interferes with the weaker ICl system. Using this approach, we observed no $I_2$ interferences.

The fluorescence observation chamber was constructed from a brass block that contained LIF observation windows and sidearms for the introduction of the dye laser beam. Light collection and focusing of the fluorescence onto the entrance slit of the monochromator was accomplished using a system of aspheric and spheric lenses. The f-number of the imaging system was carefully matched to that of the monochromator to maximize both throughput and resolution.

We completed data collection for the ICl molecule during this reporting period, and have concentrated recently on the data analysis and interpretation. The IF and ICl data collection sets and scope of the study are summarized in Tables 1 and 2 .

Table 1. Summary of the Rotational Energy Transfer Processes and Collision Partners Studied for the IF Molecule.

| J' Level Excited | Excitation Band | Observed Band | Bath Gases |
|---|---|---|---|
| 13 | 6, 7 | 6, 0 | He, Ar, Xe |
| 27 | 6, 7 | 6, 0 | He, Ar, Xe |
| 35 | 6, 7 | 6, 0 | He, Ar, Xe |
| 72 | 6, 0 | 6, 0 | He, Ne, Ar, Kr, Xe, $N_2$, $CF_4$ |
| 13 | 6, 7 | 5, 0 | He, Kr |
| 72 | 6, 0 | 5, 0 | He, Kr |

Table 2. Summary for the R-T Transfer Process and Collision Partners Studied in IC1(B)

| J' Level Excited | Excitation Frequency ($cm^{-1}$) | Observed Band | Bath Gases |
|---|---|---|---|
| 11 | 17095.24 | 1-7 | IC1 |
| 19 | 17095.04 | 1-7 | IC1 |
| 22 | 17080.29 | 1-7 | He, Ar, IC1 |
| 26 | 17088.26 | 1-7 | CO, HF |
| 27 | 17075.48 | 1-7 | He, Xe, Kr, $O_2$ |
| 35 | 17075.24 | 1-7 | He, Xe, Kr, $O_2$ |
| | | | He, Ar, IC1 |
| 36 | 17073.51 | 1-7 | IC1, CO, HF |
| 40 | 17065.99 | 1-7 | IC1 |
| 42 | 17043.50 | 1-8 | He, Ar, IC1 |
| 55 | 17029.44 | 1-7 | He, Ar, IC1 |
| 56 | 17001.89 | 1-7 | He, Xe, Kr, $O_2$ |
| 57 | 16998.47 | 1-7 | IC1 |
| 60 | 17014.32 | 1-7 | IC1, CO, HF |
| 61 | 16984.22 | 1-7 | Kr, IC1 |
| 70 | 16979.66 | 1-7 | He |
| 70 | 16979.66 | 1-8 | He, Xe, $O_2$ |
| 78 | 16947.62 | 1-7 | IC1 |

One particularly interesting aspect of the ICl results was the observation of efficient rotational energy transfer when ground state ICl is used as a collision partner for the ICl(B). As we discuss below, this effect also needs to be taken into account in the data reduction for R-T transfer when other species are used as collision partners.

B.2 Data analysis for determination of R-T rate coefficients.

The determination of R-T rate coefficients was based upon a steady state kinetic analysis. In dilute conditions where a fluorescing molecule experiences on average only a single collision during its lifetime, the steady state expression for the population of the final state is given by Eq. (1):

$$\frac{d[J_f]}{dt} = [J_i][M]k(i \rightarrow f) - \frac{[J_f]}{\tau} = 0 \quad . \tag{1}$$

This equation can be rearranged to give the working expression used to derive the R-T rate coefficients:

$$\frac{[J_f]}{[J_i]} = [M]k(i \rightarrow f)\ \tau \tag{2}$$

where $[J_i]$ and $[J_f]$ are the relative populations of the initial and final states, k(i-f) is the rate coefficient for the transfer from $J_i$ to $J_f$, and $\tau$ is the effective lifetime of $J_f$. When the single collision assumption is valid, a Stern-Volmer plot of $[J_f]/[J_i]$ versus [M] will be linear in [M] and the slope will be proportional to the R-T rate coefficient. In our experiments, care was taken to avoid bath gas pressures that were high enough to produce multiple collisions. Within the inherent scatter of the data, linear plots Stern-Volmer plots were always observed in this work. Previously[1], we presented a detailed discussion of multiple-collision effects and the tests that we use to check for such effects. We do not repeat them here.

The effective lifetime in Eq. (2) is given by:

$$\tau = \frac{1}{k_R + (k_q + k_v)[M] + k_p} \tag{3}$$

where $k_q$, $k_p$, $k_v$, and $k_R$ are the respective rate coefficients for electronic state quenching by the collision partner, predissociation, vibrational energy transfer, and radiative decay. Many of these rate coefficients are known or are negligible for IF(B) and ICl(B). For example, electronic state quenching of IF(B) by the noble gases, $CH_4$, and $N_2$, has been measured and is uniformly inefficient[2]. The effects of quenching by the bath gases were thus minor in these experiments, but were nonetheless included. Vibrational transfer was accounted for using the rate coefficients measured for IF(B) in collision with the noble gases and $N_2$ by

Wolf and Davis[3]. Under the conditions of these experiments, the vibrational transfer rates were always less than 10% of the IF(B) radiative rate.

Predissociation in the B states of IF and ICl have been exhaustively studied previously and there are vibrational levels within the B states of these molecules that are completely stable. Girard et al.[4] have shown that, for $v' = 6$, the vibrational level excited in all experiments involving IF(B), all $J' < 120$ are stable and do not collisionally predissociate. Consequently, all $J'$ observed in this work, $J' < 85$, have similar lifetimes in the absence of collisions. We used an average lifetime for these states of 8.2 $\mu$s as measured by Clyne and McDermid[5].

In the case of IF(B), the effective lifetime expression was modified to include the effects of quenching by any $I_2$ present in the fluorescence cell. Typically, the rate for quenching by molecular iodine was less than 10% of the radiative rate for the IF (B-X) emission.

In the ICl experiments we excited several selected rotational levels in ICl(B,$v'=1$). It has been shown[6-8] that the $v'=1$ rotational manifold is completely stable with respect to predissociation. We used the radiative rate of 4.2 $\mu$s as determined by Kitimura et al.[7] There are no rate coefficients available for vibrational energy transfer and electronic state quenching for the collision partners that we studied. However, for the results reported here we used rare gas collision partners. Electronic quenching of the B states of other interhalogens such as IF, BrCl, and BrF by rare gases is uniformly inefficient. Indeed, at the low bath gas pressures used in this work, electronic quenching is negligible. Determination of rate coefficients for electronic quenching was beyond the scope of the present program. Consequently we have assumed that the electronic quenching by the rare gases is negligible for the present ICl studies. Likewise, we have assumed rate coefficients for V-T relaxation are the same as the corresponding quantities for IF(B) for all bath gases used. We also emphasize that when values for these rate coefficients become available these data can be incorporated into our data sets. We would expect only a minor modifications of our reported values for the R-T rate coefficients. All the observed trends for the R-T rate coefficients with respect to $\Delta J$ are independent of these other processes.

Unlike the experiments involving IF(B), the ICl pressure could be systematically varied and determined with a capacitance manometer. Thus we could study the effects of ICl-ICl collisions. Although this was fundamentally interesting, it also allowed a more accurate determination of rate coefficients for ICl with other collision partners. We were able to account for any R-T transfer caused by ICl even in the presence of a large excess of bath gas such as helium. In the course of the ICl experiments, we found that as the bath gas pressure in the fluorescence chamber was increased there was a concomitant decrease in the ICl pressure. This was due to the low ICl vapor pressure over the $ICl_3$ crystals. In effect, higher bath gas pressures hindered transport by diffusion of the ICl vapor from the ICl source cell to the observation chamber. We note that this was not a problem in the IF experiments since the $I_2$ was contained in a saturator, this allowed us to keep the $I_2$ vapor pressure in the fluorescence cell constant. Recall that the $I_2$ was the source of IF in those experiments.

We modified our data reduction routines for the ICl data to account for the self transfer. This represents an important addition to the data analysis since we found that ICl has much larger rate coefficients for RET than other collision partners we have investigated. As a result, ICl + ICl collisions have an important effect on the determination of R-T rate coefficients with other collision partners.

The presence of ICl in the gas mixture leads to corrections due to self-quenching, vibrational transfer, and R-T transfer. The corresponding effective lifetime for ICl(B) is then given by:

$$\tau = \frac{1}{k_R + k_p + \left(k_q^M + k_v^M\right)[M] + \left(k_q^{ICl} + k_v^{ICl}\right)[ICl]} \quad . \tag{4}$$

This results in a modified Stern-Volmer expression:

$$\frac{[J_f]}{[J_i]} - k_R^{ICl}(i \rightarrow f)\,[ICl] \cdot \tau = k_R^M (i-f)[M] \cdot \tau \tag{5}$$

where $k_R^{ICl}(i \rightarrow f)$ is the rate coefficient for R-T transfer due to ICl(B) colliding with ICl. We employed the value of $2.1 \times 10^{-10}$ cm$^3$ molecule$^{-1}$ s$^{-1}$ for $k_q$ as determined by Kitimura et al.[8]

In order to apply Eq. (5), the rate coefficients for $k_R^{ICl}$ must be determined. We used the initial Stern-Volmer analysis described above with ICl as the collision partner for the determination of rate coefficients for self R-T transfer out of several initially excited rotational levels in ICl(B,v'=1): $J_i$ = 61, 57, 39, and 35. The resulting rate coefficients were somewhat scattered, consequently, they were both averaged and smoothed prior to use in Eq. (5). The coefficients from $J_i$=57 and 61 were smoothed and averaged and then used to correct the data from other collision partners where $J_i \geq 56$. A similar procedure was employed for the coefficients from $J_i$ = 35 and 39 and the resulting coefficients were used to correct the data from $J_i \leq 36$ for other bath gases. Figure 2 shows a set of smoothed coefficients. These rate coefficient sets were used to modify the population ratios $[J_f]/[J_i]$ by means of Eq. (5). In Figure 3 we present an example of the effect of this treatment for the case of ICl + Kr collisions. Both the uncorrected rate coefficients and those corrected for self transfer are shown.

B.3 Spectral fitting.

The relative populations of the initial and final states used in Eqs. (2) and (5) were measured using the intensities of the respective P- and R-branch transitions from these levels (there are no Q-branch transitions due to symmetry restrictions). The relationship between the relative intensities and relative populations is given in Eq. (6):[1]

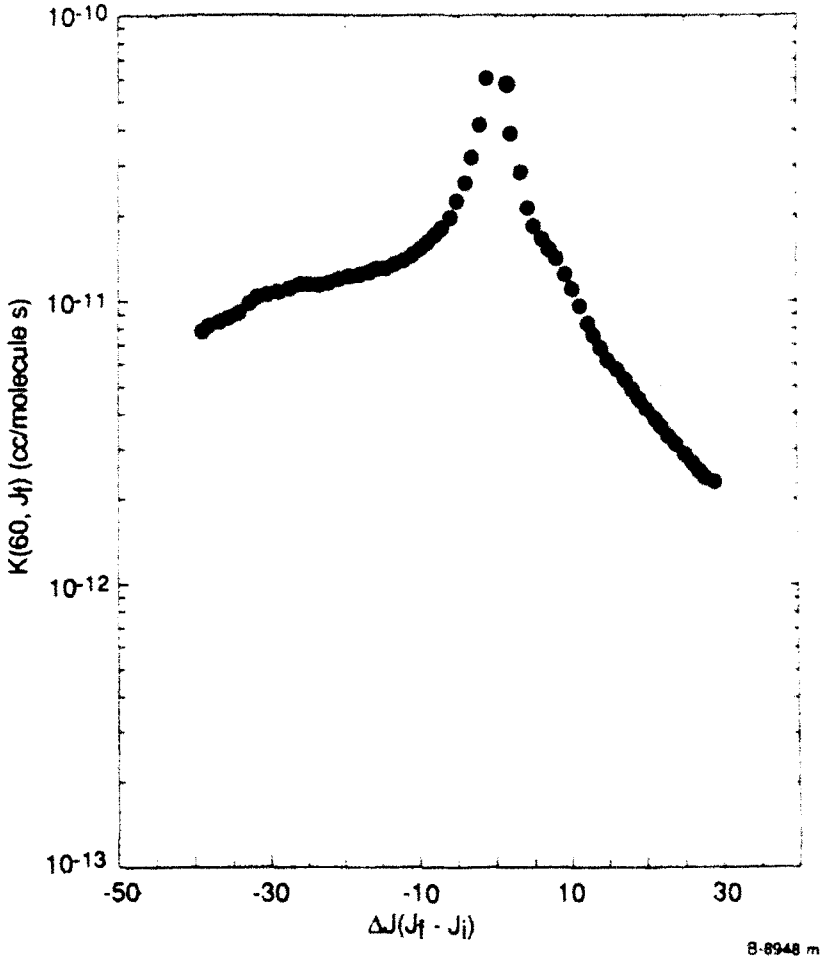


Figure 2
Distribution of R-T Rate Coefficients for Self Relaxation by ICl. The data have been smoothed as described in the text. These data were applied in the determination of rate coefficients for RET due to other collision partners where $J_i \geq 56$.

$$I_{J',J''}^{v',v''} = N_{J'}^{v'} \nu^3 \cdot |Re|^2 q_{v',v''} \left( \frac{S_{J',J''}}{2J'+1} \right) \tag{6}$$

where $S_{J',J''}$ is the rotational linestrength, $\nu$ is the transition frequency, Re is the electronic transition moment, and $q_{v',v''}$ is the Franck-Condon factor.

The relative intensities in Eq. (6) can be determined either by measuring the peak intensities or the integrated intensities of the corresponding transitions. Since the spectral resolution available to us was insufficient to completely resolve all the observed transitions, we measured integrated intensities from each J' using a spectral fitting program that allows the

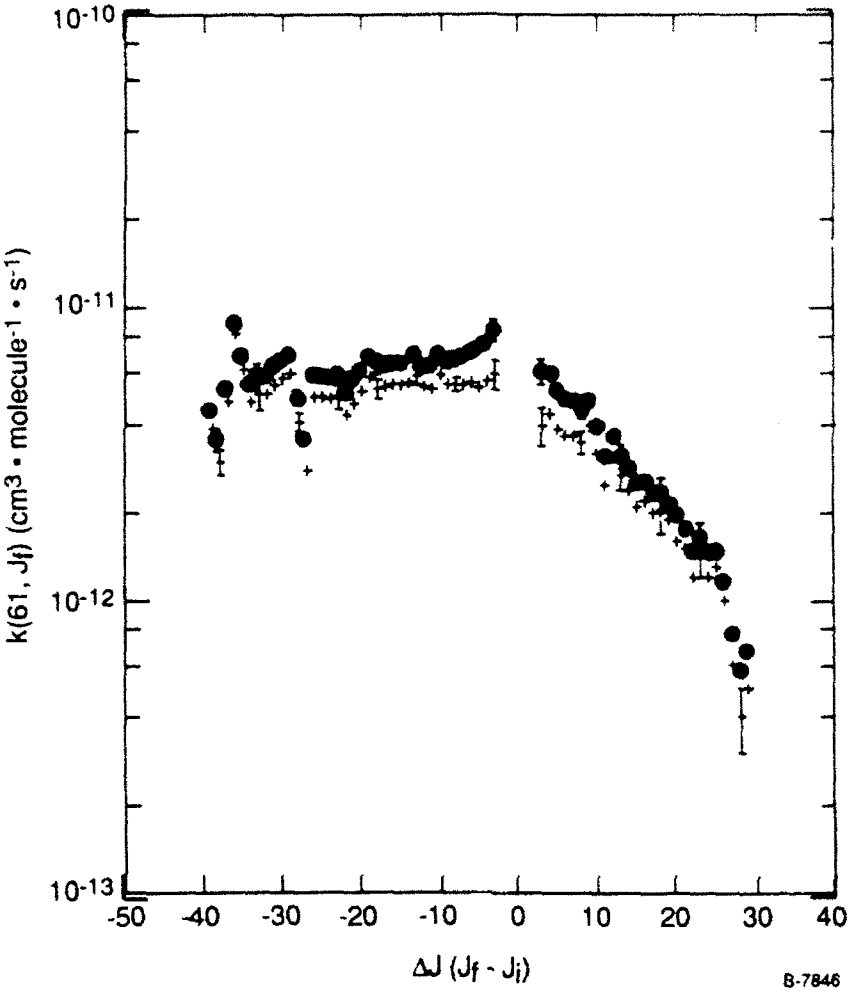


Figure 3
Comparison of R-T Rate Coefficients That Have Not Been Corrected for Self Transfer (+) to Those That Have Been Corrected (●) Using the Treatment Described Above. Collision partner was krypton.

determination of populations from dispersed fluorescence spectra even when substantial overlap occurs. The spectral fitting procedure is described in detail in Ref. 1.

We have consistently observed a bleed over on the diode array for pixels immediately adjacent to those illuminated by the relatively intense radiation from transitions originating from the parent $J_i$. This made accurate determination of populations for nearby $J_f$ difficult. Consequently, we have not included levels immediately adjacent to the $J_i$ in the data analysis. We feel that this is an inherent difficulty when using a diode array detector. However, the advantages in data collection efficiency far outweigh this slight deficiency.

We also found that the fitting code would calculate populations for levels radiating in regions of the spectrum where there is severe overlap, e.g., near the bandhead. The populations

determined under these conditions do not always vary smoothly from one rotational level to the next, particularly if the signal to noise in the fluorescence spectrum is poor. This was largely responsible for much of the scatter in the data from lower $J_f$ with IF(B).

The spectral constants of Trickl and Wanner[9] were employed for the fitting of the IF spectra. The constants are in the Dunham expansion format and were found to give extremely accurate line positions. Indeed it was found that the ring laser could be tuned to any desired transition using the calculated line positions and the wavemeter.

The spectral constants of Brand and Hoy[10] were used for ICl(X) and those of Clyne and McDermid[7] were used for ICl(B). Both sets of spectral constants are considerably less extensive and refined than those used to calculate the IF(B-X) spectra. Accurate measurement of these spectral constants, though possible with the equipment available for this program, was outside the scope of this effort. Deficiencies in the constants manifest themselves as a "dephasing" of the calculated and observed rotational lines at large displacements from the originating from the initially pumped rotational level. This was primarily a problem with the data from the lower rotational levels ($J_i \leftarrow 40$) since larger positive $\Delta J$ transfer is possible with these levels. Because of this difficulty, rate coefficients from these data are somewhat less reliable and were not used in the testing of the fitting laws.

B.4 The fitting laws.

We have tested a single variant of each of four laws that describe rotationally inelastic energy transfer in an attempt to determine simple closed form expressions for the rate coefficient matrix describing RET in these systems. The exponential gap law (EGL) and the statistical power gap law (SPG) scale the calculated rate coefficients with the rotational energy change resulting from the collision. The energy corrected sudden law (ECS) and the infinite order sudden law (IOS) scale the rate coefficients with the angular momentum exchanged during the collision. These fitting laws are described in detail in Refs. 11 through 13.

The exponential gap law (EGL) is the oldest fitting law and was originally proposed by Polanyi and Woodall[14] to account for RET resulting from HF-HF collisions. This law has been subsequently shown to be consistent with surprisal theory (Ref. A and references therein) and is given by:

$$k^{EGL}_{(i\rightarrow f)} = a \cdot e^{-(\Theta|\Delta E_{ROT}|)} \cdot R(\Delta E) \cdot (2J_f+1) \qquad (7)$$

where a and $\Theta$ are the fitted parameters, $\Delta E$ is the difference in rotational energy between $J_i$ and $J_f$, and $R(\Delta E)$ is the ratio of final to initial translational state densities. Inclusion of the term $2J_f + 1$ corresponds to the assumption that all final $m_J$ states are accessible in the collision.

The statistical power gap law (SPG) was originally proposed by Brunner et al.[15] to account for RET in collisions between $Na_2$ and Xe and has since been applied with some success to data from $Na_2$ in collision with additional bath gases[13] and $I_2$ in collisions with He and Xe[16]. This law differs from the exponential gap law in that rate coefficients scale as a power of the energy difference. It is given by:

$$k^{SPG}_{(i\rightarrow f)} = a \cdot \left|\frac{\Delta E_{ROT}}{B_v}\right|^{\alpha} \cdot N_{\lambda}(J_{i,}J_f) \cdot (R(\Delta E) \tag{8}$$

where a, $\alpha$, and $\lambda$ are the fitted parameters and $B_v$ is the rotational constant. We have employed a version of this law that allows restrictions to be placed on $\Delta m_J$. These restrictions are contained in the factor $N_\lambda$ and are determined by the parameter $\lambda$. This provision allows limits on the relative spatial orientation of the rotating molecule before and after a collision. When lambda exceeds $J_i + J_f$, $N_\lambda$ reaches a limiting value of $2J_f + 1$ and there is no longer a restriction in $\Delta m_J$.

The energy-corrected sudden law was originally proposed by DePristo et al.[17] and arises from the sudden approximation of inelastic scattering theory. It has been applied with success to RET in several systems[11-13,18]. This law is given by:

$$k^{ECS}(J_i\rightarrow J_f) = (2j_f + 1)\exp\left[\left(E_{J_i} - E_{J>}\right)/kT\right]$$
$$\times\left[\sum\begin{bmatrix} j_i & j_f \\ 0 & 0 \end{bmatrix}^2 (2\ell + 1)\begin{bmatrix} j> \\ A \\ \ell \end{bmatrix} k(\ell\rightarrow 0)\right] \tag{9}$$

where the term in brackets is a 3-j symbol, J> is the larger of $J_i$ and $J_f$, and the sum over $\ell$ ranges from $|J_i - J_f|$ to $|J_i + J_f|$. The k(l→0) are referred to as basis rate coefficients and describe transfer out of $J_i = 0$. In principle these quantities can be measured, however such measurements present substantial difficulties (e.g., isolating a transition populating J = 0 and resolving the resulting fluorescence). Consequently, like other investigators, we employ one of several analytic forms, in this case given by Eq. (10):

$$k(\ell\rightarrow 0) = \alpha[\ell(\ell+1)]^{-\gamma} \tag{10}$$

where $\alpha$ and $\gamma$ are the variable parameters. This form for the basis rate coefficients has been successfully used to fit rate coefficients from the $I_2(B)$ + Xe, He,[16] and $Na_2(A)$ in collisions with several gases.[13] The term $A_{J>}$ is an adiabatic correction allowing for molecular rotation during the collision and is given by:

$$A_\ell^{J>} = \frac{1 + \tau_\ell^2/6}{1 + \tau_{J>}^2/6} \tag{11}$$

where $\tau_J$ is a reduced collision duration given as the number of radians rotated by the molecule during the collision ($\tau_J = \omega_J \times T_d$). The collision duration $T_d$ is equal to $l_c/v$ where $l_c$ is an average effective collision length and v is the mean closing velocity of the collision pair. Along with the terms in the basis rate coefficients, $l_c$ can be varied in order to best fit the data.

The infinite order sudden (IOS) law is a simplification of the energy corrected sudden law where the effective collision length is assumed to be zero. The expression for the infinite order sudden law as applied in this analysis is given by Eq. (9) where the adiabatic correction term $A_{J>}$ is now unity. This law would be expected to be most appropriate for collisions with light, fast moving collision partners which are more likely to produce short impulsive collisions.

The fitting of data was performed using a non-linear least squares program based on the Levinburg-Marquardt method as found in Bevington[19]. This is a rapidly converging algorithm which attempts to produce a "best fit" by minimizing the reduced chi square function given by:

$$\chi^2 + \sum_{J_f} = \frac{[(k_{fit}(i \rightarrow f) - k_{expt}(i \rightarrow f))]^2}{\sigma^2(i \rightarrow f)} \tag{12}$$

where $\nu$ is the number of independent degrees of freedom in the fit (number of experimental data points minus the number of fitted parameters) and $\sigma$ are the individual errors associated with the rate coefficients. For the $\sigma$ we used the errors produced by the least squares fitting routine used to determine the rate coefficients. These are also chi square functions describing the deviation of the experimental population ratios from the best fit line giving the rate coefficient.

Data from all $J_i$ for a given collision partner were used simultaneously in a global fit. We present two figures of merit to judge the quality of the fit: the reduced chi-square and the average percent deviation between the calculated and experimental rate coefficients.

B.5 Visible optically-pumped laser.

In an effort to demonstrate further the potential of the interhalogens as visible laser candidates, we completed a study in which we attempted to produce an optically-pumped ICl (B-X) laser. The apparatus for this study is shown in Figure 4. The excitation source was a

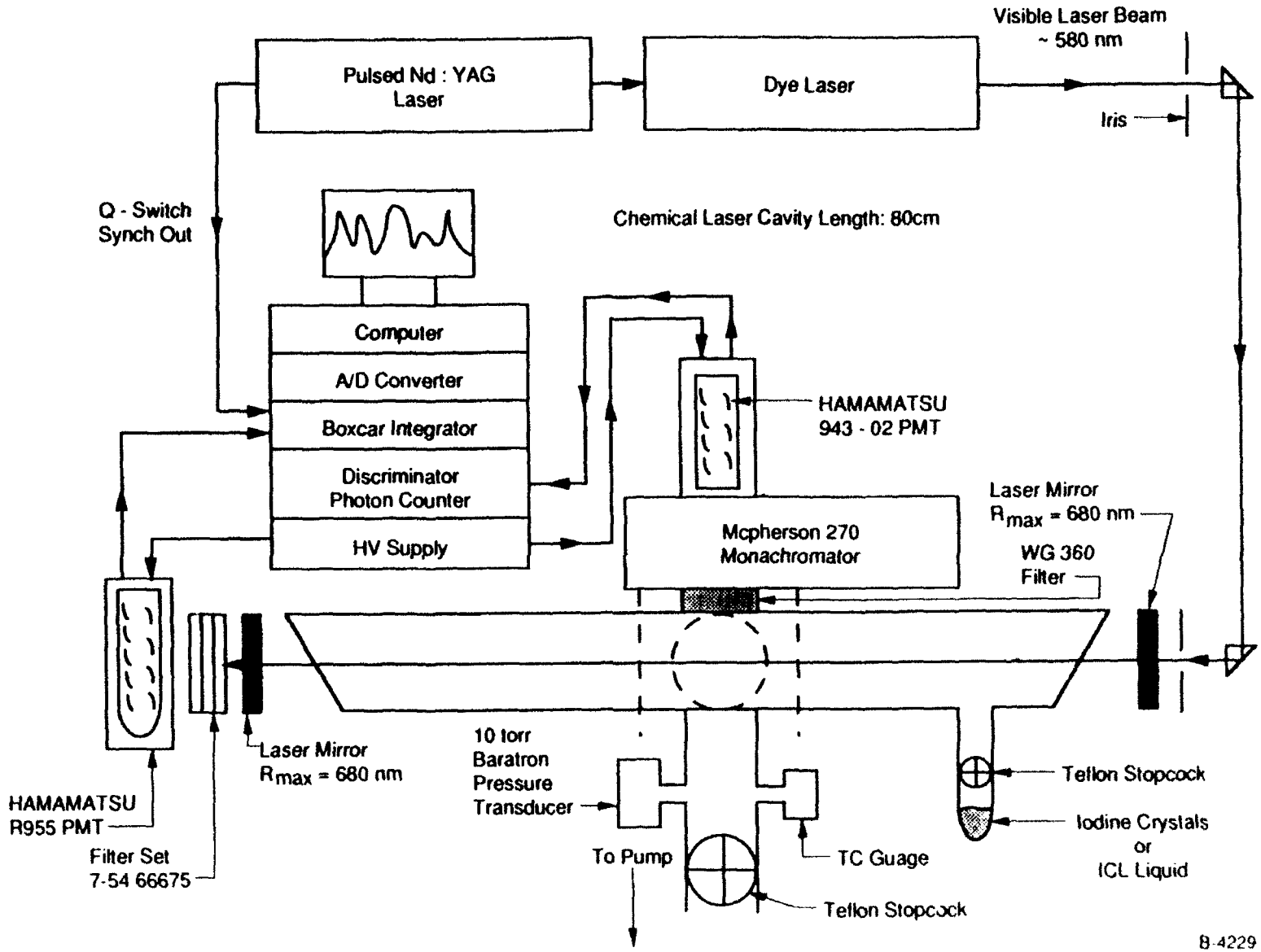


Figure 4
Apparatus for the ICl Optically-pumped Laser Study.

Quantel Nd:YAG laser pumped dye laser. A mix of LD 590 and LD 610 laser dyes (Exciton) was used to produce output energies in excess of 10 mJ over the wavelength range of 580 and 610 nm. The selection of the excitation wavelengths for the ICl depend critically upon the Franck-Condon factors for absorption and the stability of the ICl B-state manifold. Since all the levels $v' > 3$ are predissociated, only a rather limited range of excitation schemes are available. In Table 3 we list the excitation bands considered and indicate the relative absorption strengths (product of the relative population and the Franck Condon factor).

Table 3. ICl (B→X) Bands used in the OPL Studies

| $v',v''$ | $q_{v',v''}$[a] | $\Theta_{v''}$[b] | $q_{v',v''} \bullet \Theta_{v''}$ |
|---|---|---|---|
| 0,0 | $8 \times 10^{-7}$ | 0.84 | $6.7 \times 10^{-7}$ |
| 1,0 | $6 \times 10^{-6}$ | 0.84 | $5.0 \times 10^{-6}$ |
| 2,0 | $2 \times 10^{-5}$ | 0.84 | $1.7 \times 10^{-5}$ |
| 1,1 | $9 \times 10^{-5}$ | 0.13 | $1.1 \times 10^{-5}$ |
| 2,1 | $3 \times 10^{-4}$ | 0.13 | $3.9 \times 10^{-4}$ |
| 2,2 | $2 \times 10^{-3}$ | 0.02 | $4 \times 10^{-4}$ |

[a]Franck Condon factor.
[b]Relative v" population of 300 K.

B.6 "$O_4$ laser" support.

We have been following closely the reports of $O_4$ lasing in chemically-generated oxygen. The work by Yoshida et al.[20] attributed visible wavelength emissions to the $O_4$ molecule. We were intrigued by the report of lasing in a species such as $O_4$, which has an extremely high predissociation rate but a relatively small radiative rate. Indeed, the collisional nature of $O_4^*$ would make lasing extremely difficult to obtain.

The spectra reported by Yoshida et al.[20] are reproduced in Figure 5. In a search for other possible sources for this emission we considered the well known $Cl_2(B \rightarrow X)$ emission system. Molecular chlorine is the primary gaseous "fuel" in a chemical oxygen generator. Although the generators are typically run under conditions where the $Cl_2$ is completely consumed the existence of $Cl_2$ in the $O_2$ flow has been observed previously.

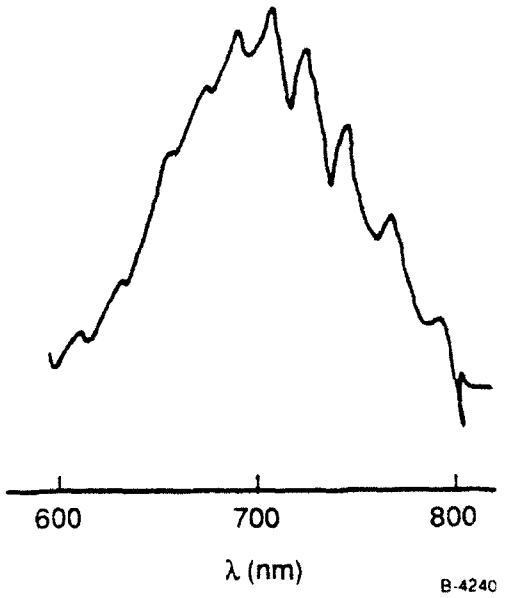


Figure 5
"$O_4$" Spectrum (from Yoshida et al.)[20]

B.7 Ground state relaxation in the ground state of IF.

For electronic transition laser applications, relaxation within the ground electronic is an important process. In many laser systems, relaxation out of the terminal rotational level will be rate limiting in the limit of high power operation, i.e., for large stimulated emission rates bottlenecking will occur. In previous optically pumped IF laser studies, we saw evidence of this phenomenon in high power operation of the IF laser. Since rotational relaxation is usually much faster than vibrational relaxation, it is the most important in terms of bottlenecking.

Vibrational relaxation within the ground electronic state can also play an important role in some energy transfer excitation schemes. For example, Davis and Woodward[21] have shown that population within high vibrational levels of IF(X) significantly enhance the production rate of IF(B) in the presence of $O_2(a)$. This internal vibrational energy apparently opens energy transfer pathways that otherwise would be inaccessible. The immunity of these vibrational levels to electronic quenching will be important in any pressure scaling of the IF laser. Consequently, we have made preliminary measurements of vibrational relaxation of selected levels within the ground electronic state.

These measurements were performed on the apparatus shown in Figure 6. The IF(X,v) was produced by reacting either ICl or $I_2$ with F atoms. As indicated in Figure 6, the fluorine atoms were produced by passing a flow of helium and $CF_4$ through a microwave discharge

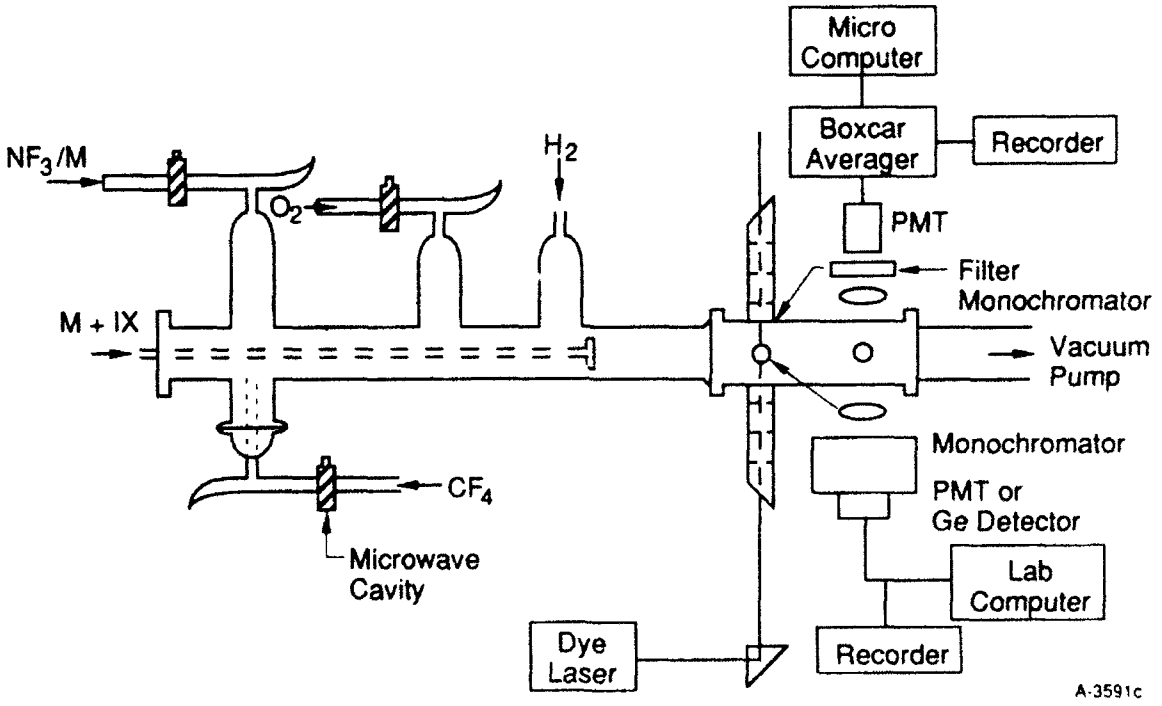


Figure 6
Apparatus Used for the Initial Studies of Relaxation of Ground State IF.

cavity. The reactions of ICl or $I_2$ with F are known to produce IF(X,v) with high efficiency.[22] In addition the exothermic limits of for the respective reactions are $v''=9$ and $v''=19$. Thus, we could prepare flows of IF(X,v) that could be used to study vibrational relaxation.

We monitored the relative concentration of IF(X,v) using Stokes shifted laser induced fluorescence. We note that excitation wavelengths that connect high vibrational levels in IF(X) to IF(B) are in the range 600 to 700 nm. These are conveniently produced using a dye laser. We used a pulsed, frequency doubled Nd:YAG laser as indicated in Figure 4. The LIF was detected using GaAs PMT and a narrow bandpass interference filter centered at 490 nm. This combination allowed us to probe levels $6 < v'' < 14$.

In Figure 7 we show a sample spectrum of LIF from several v″ levels. The rotational structure is partially resolved for each band observed. The intensity of each LIF band is proportional to the population within the v″ level that is excited by the dye laser. Thus, we can use the LIF spectra to determine the relative population of selected v″ levels.

As indicated in Figure 6, we used a sliding injector to introduce the ICl into a flow of F atoms and the bath gas that we wished to study. The observation port was fixed, and the distance from the injection point for the ICl and the to the observation port determined the reaction time. All observations were done far enough downstream so that mixing corrections were negligible.

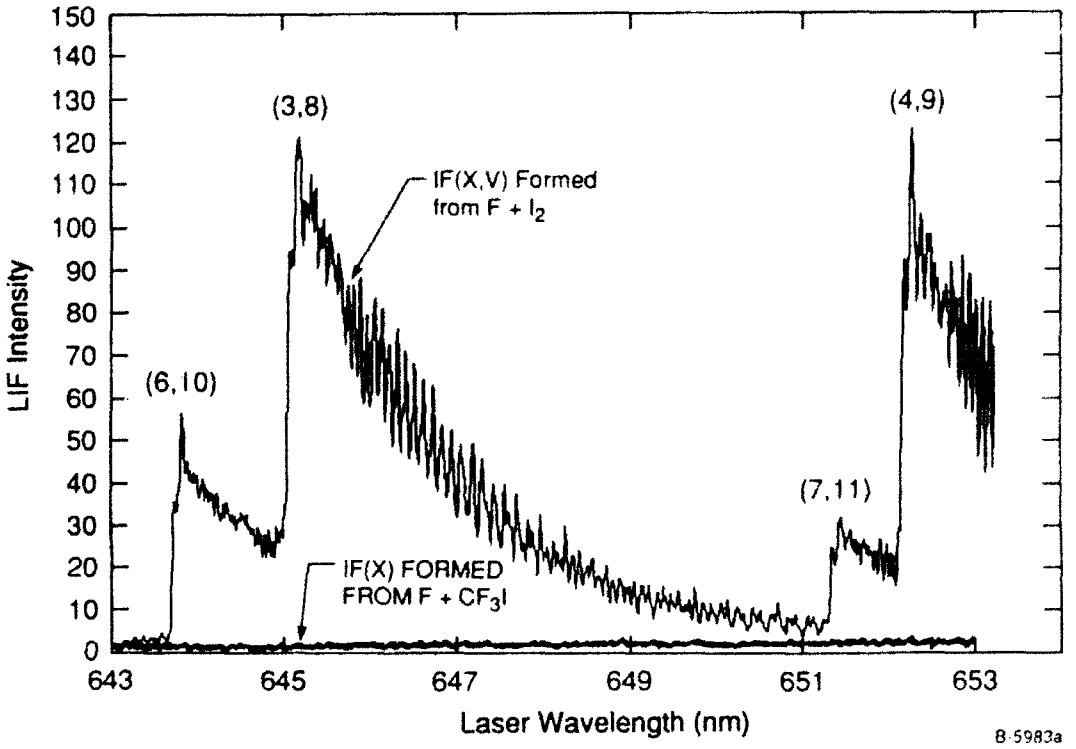


Figure 7
Excitation Spectra Showing IF(X,v) Produced from the Reactions of $I_2$ + F and $CF_3I$ + F.

In this limit the rate of decay of the initially formed IF(X,v) is given by Eq. (13).

$$\frac{\Delta[IF(x,v)]}{\Delta t} = -[IF(x,v)](k_v[M] + k_w) \qquad (13)$$

where $k_v$ is the rate coefficient for V-T relaxation and $k_w$ is the rate coefficient for deactivation of IF on the walls. The time is given by l/v where l is the distance from the injector to the observation port and v is the bulk flow velocity. In the preliminary analysis that we present here we have not included the effects of diffusion to the cell walls. Consequently, the preliminary rate coefficients that we report here represent upper limits for V-T relaxation.

B.8 Optically-pumped HF laser.

We also initiated some studies that were intended to demonstrate the feasibility of developing mid-IR lasers based upon optically-pumped gas phase species. These experiments were motivated in part by the de-emphasis of short wavelength chemical lasers by the Air Force Phillips Laboratory. There are current missions identified by the Air Force for mid-IR lasers. These include electro-optical countermeasure devices and asset defense. One promising method of producing laser output in the 3 to 5 micron wavelength range is optically-pumped gas phase species. We have performed some studies using overtone excitation in HF as a starting point for assessing this approach.

The excitation and emission scheme are indicated in Figure 8. We excited several rotational lines in both the (2,0) and (3,0) overtone bands in HF. For these experiments we used no optical resonator. Rather, we studied amplified spontaneous emission from the overtone-pumped HF. The optical gain for many diatomic molecules is expected to be high as indicated in Table 4. Consequently, ASE provides a convenient method for assessing some of the stimulated emission properties of overtone excited molecules.

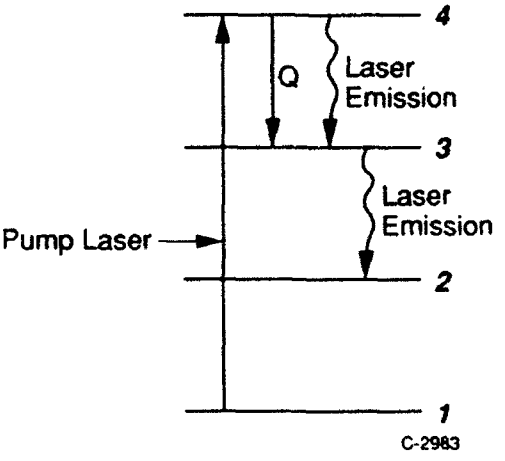


Figure 8
Energy Levels Showing Excitation and Emission in Overtone-pumped Diatomic Species.

The overtone excitation experiments on HF were performed using the apparatus shown in Figure 9. The excitation source was a Continuum TDL 50 dye laser that was Raman shifted to produce output in the 875 to 1300 nm wavelength range. The dye laser was pumped by a Continuum model 481 Nd:YAG laser that was frequently doubled. The pulse length was approximately 8 ns, and the bandwidth of the Raman shifted output was less than 0.12 $cm^{-1}$. As indicated in Figure 9

Table 4. Predicted Laser Parameters for Several Candidate Laser Systems

| Molecule | Pump Band | Apump ($\mu$m) | $\sigma_{AB}(2\leftarrow0)$ ($cm^2$) | $N_{v'J'}$ ($cm^{-3}$) | $\sigma_{SE}(2\rightarrow1)$ ($cm^2$) | Gain ($cm^{-1}$) |
|---|---|---|---|---|---|---|
| HCl | (2,0) | 1.73 | $6.4 \times 10^{-19}$ | $1.1 \times 10^{15}$ | $1.2 \times 10^{-15}$ | 1.36 |
| HF** | (2,0) | 1.32 | $2.0 \times 10^{-18}$ | $4.9 \times 10^{15}$ | $1.9 \times 10^{-15}$ | 9.2 |
| DF** | (2,0) | 1.78 | $9.1 \times 10^{-19}$ | $2.1 \times 10^{15}$ | $1.4 \times 10^{-15}$ | 6.9 |
| CO† | (2,0) | 2.7 | $4.0 \times 10^{-19}$ | $7.8 \times 10^{14}$ | $1.2 \times 10^{-15}$ | 0.94 |
| Assuming 10 Torr of species, 2 mJ/10 ns laser pulse, beam diameter 6 mm, and pump laser bandwidth of 0.1 cm | | | | | | |

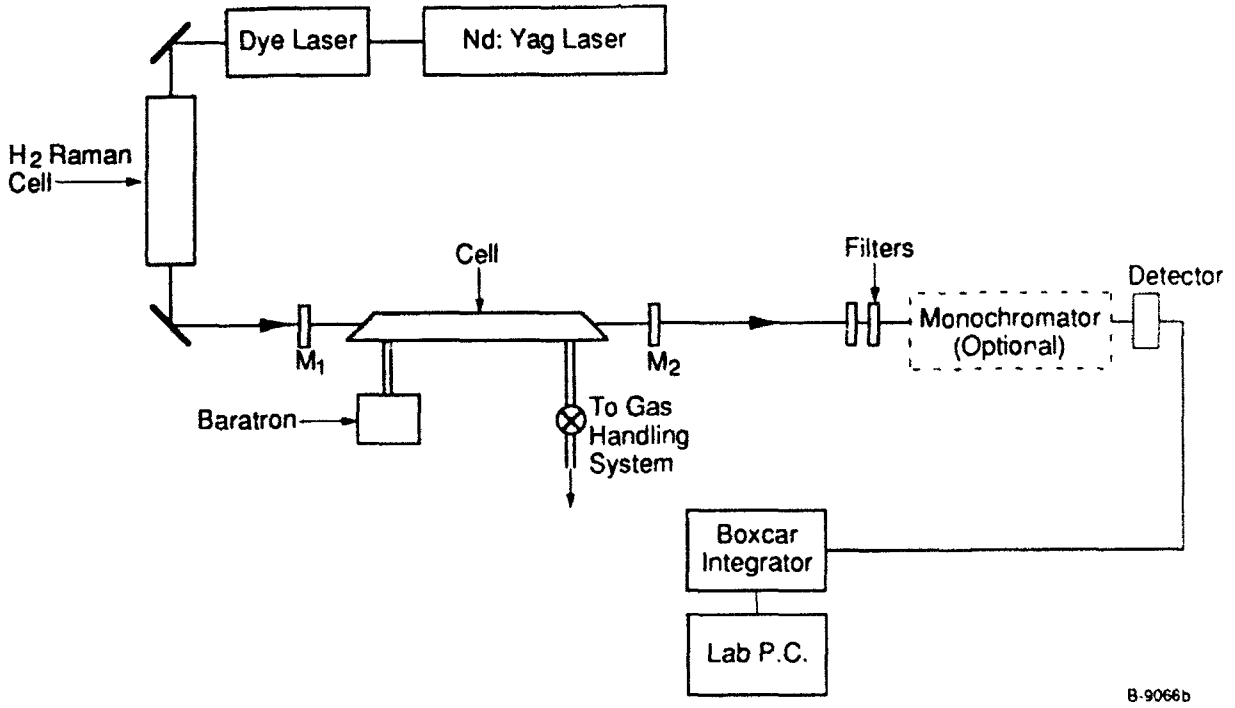


Figure 9
Block Diagram of Apparatus Used in the ASE Experiments.

the HF cells were excited longitudinally. We used two cells, one was 112 cm long and the second cell was only 7.5 cm long. The cells were connected to a passivated gas handling system and were pumped to less than 0.1m Torr prior to filling. Cells were filled with neat HF or with mixtures of HF and He. Detection of both absorbed pump radiation and the HF ASE were accomplished using a liquid nitrogen-cooled InAs detector. A series of long pass and short pass optical filters were used to isolate the ASE emission. For some studies a

0.3m monochromator was used to spectrally resolve the ASE in order to study energy transfer within the excited HF.

Prior to ASE tests the HF cell was placed in a Shimadzu model 3000 spectrophotometer and we obtained absorption spectra for overtone transitions. A typical trace is shown in Figure 10.

The actual HF overtone ASE tests were performed using the following approach. First the cell was excited with the Raman shifted dye laser operating at low power. We monitored the transmitted pump power as a function of the excitation wavelength and obtained absorption spectra. Following this, the dye laser was tuned to a particular absorption line and a long pass filter was placed in front of the InAs detector to prevent the Raman shifted dye laser radiation from impinging on the detector. The dye laser power was increased and searches for stimulated emission on HF fundamental bands near 2.7 microns were initiated. For many experiments the dye laser wavelength was scanned and we monitored broadband ASE.

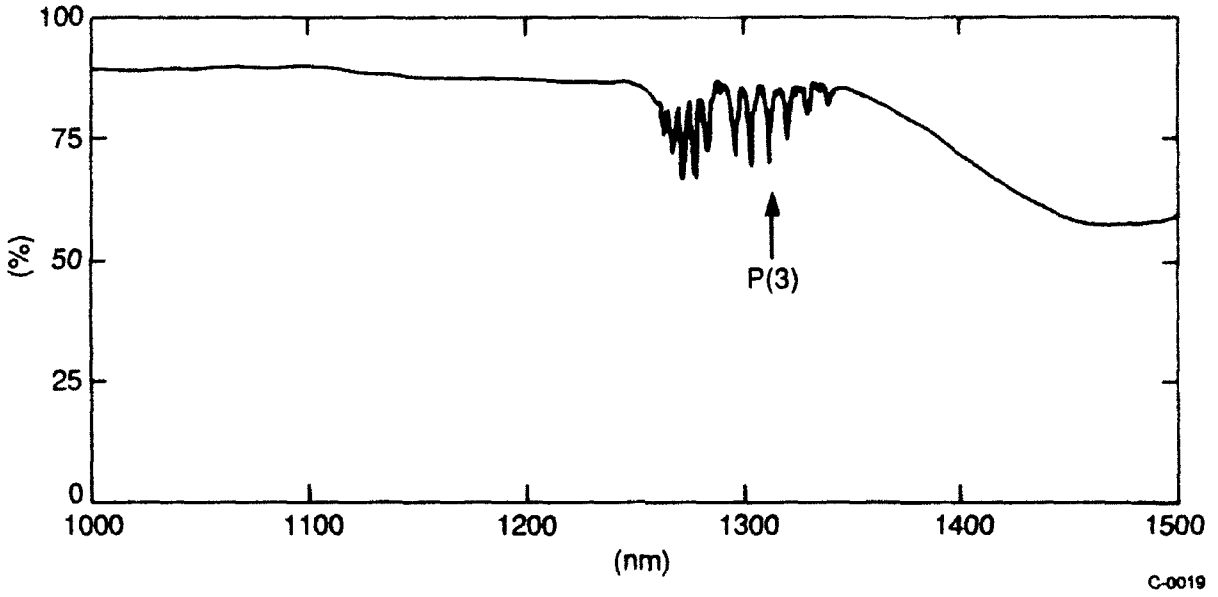


Figure 10
Absorption Spectrum of HF (2,0) Band in a 7.5 cm Long Cell.
These data were obtained using a spectrophotometer.

## C. Results

### C.1 R-T rate coefficients for ICl.

Sample data for ICl R-T transfer using oxygen as the collision partner is shown in Figure 11. The $O_2$ pressure is shown, and we see clearly the effects of R-T transfer. In Figures 12a and 12b we present Stern-Volmer plots of equation from which the R-T rate coefficients are

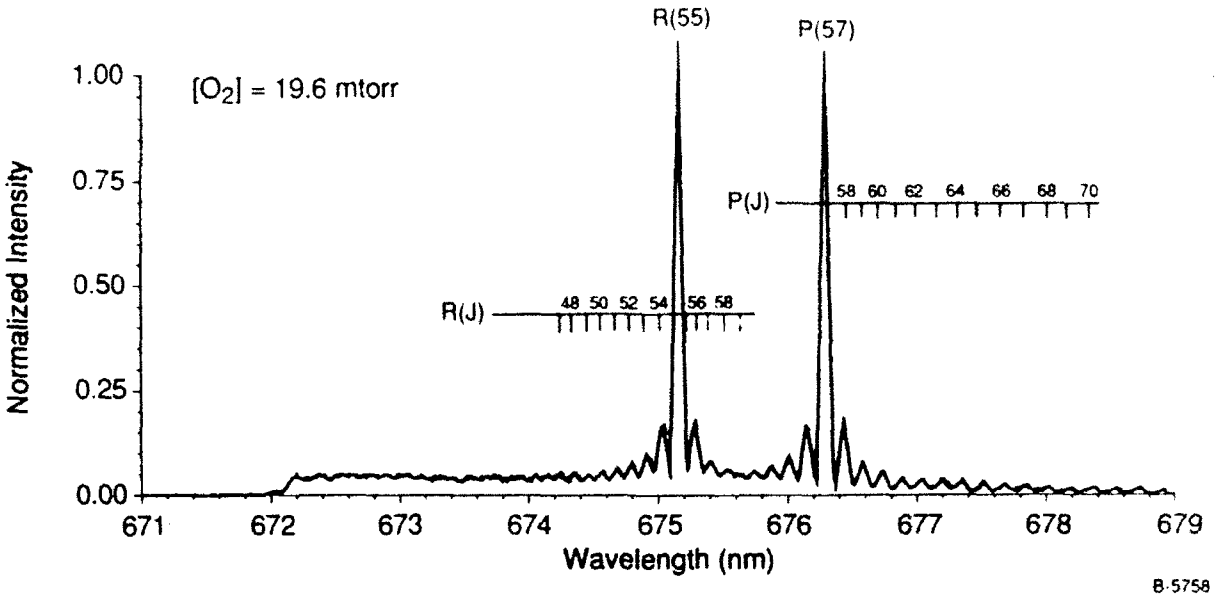


Figure 11
Resolved ICl (B→X) Fluorescence on the (1, 7) Band.
The dye laser initially excited $J'=56$ in $v'=1$. Rotational relaxation by $O_2$ is shown.
Light line is data; dark line is spectral fit to the data.

determined. Two processes are shown: one for transfer to a higher rotational level (extraction of energy from the bath gas) and transfer to a lower rotational level (addition of energy to the bath gas). The rate coefficients for these processes are indicated in Figure 12.

In Figure 13 we present a distribution of R-T rate coefficients for as a function of the number of rotational quanta exchanged in the collision using ICl as the collision partner. Inspection of Figure 13 reveals two distinct regions: a strong peak for small $\Delta J$ and a much broader distribution for larger $\Delta J$. This strong propensity for small $\Delta J$ is the most striking that we have observed in all of our investigations. In addition the absolute magnitude of the small $\Delta J$ rate coefficients are a large fraction of gas kinetic. Indeed, the sum of the individual rate coefficients (the rate coefficient for R-T removal from the initially excited level) is on the order of $10^{-9}$ $cm^3$ $molecules^{-1}$ $s^{-1}$. This is a factor of three larger than any other R-T rate coefficient that we have observed in IF, BrCl, or ICl. We suggest that long range dipole-dipole interactions from ICl + ICl collisions may be responsible for this behavior. The rate coefficients that we have determined for ICl collisions with several bath gases are presented in an Appendix.

In Figures 14 through 16 we present comparisons of fitting laws to data for ICl collisions with several bath gases. We note that as the mass of the collision partner increases, the distribution becomes less peaked about small $\Delta J$. This is similar to the behavior that we observed for IF and is analogous to that reported previously for $I_2$.[16]

In Tables 5 and 6 we compare the four fitting laws for both IF and ICl.

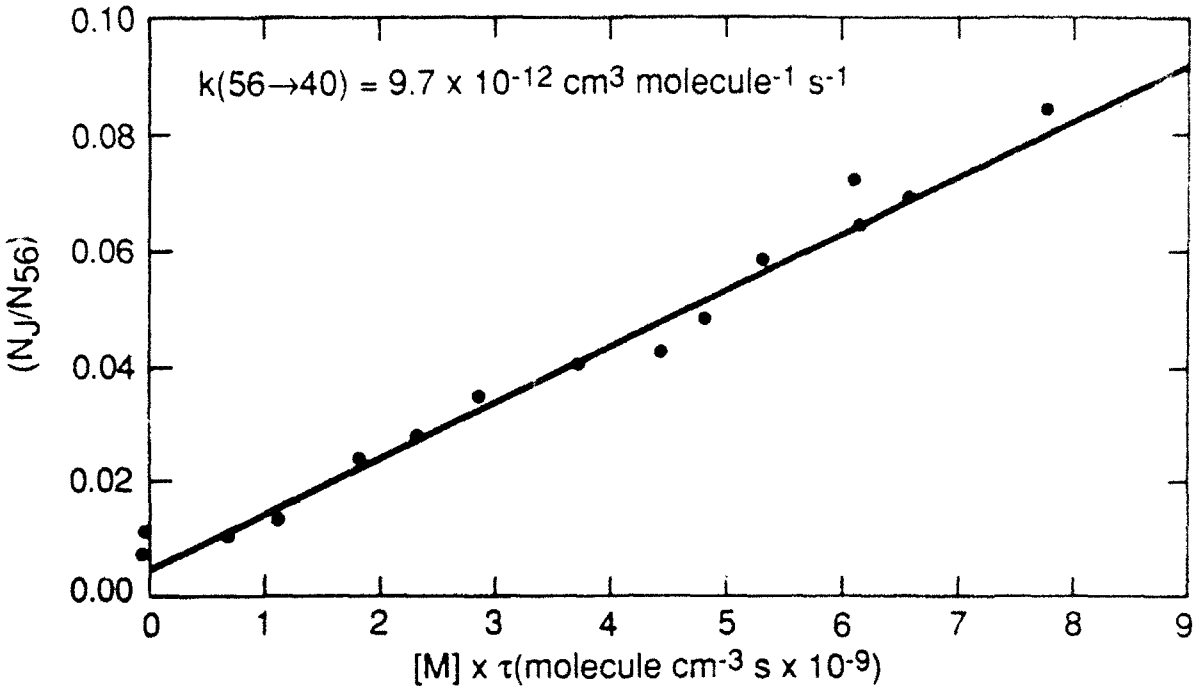


a) Stern-Volmer plot for relaxation from $J_i = 56 \rightarrow J_i = 40$

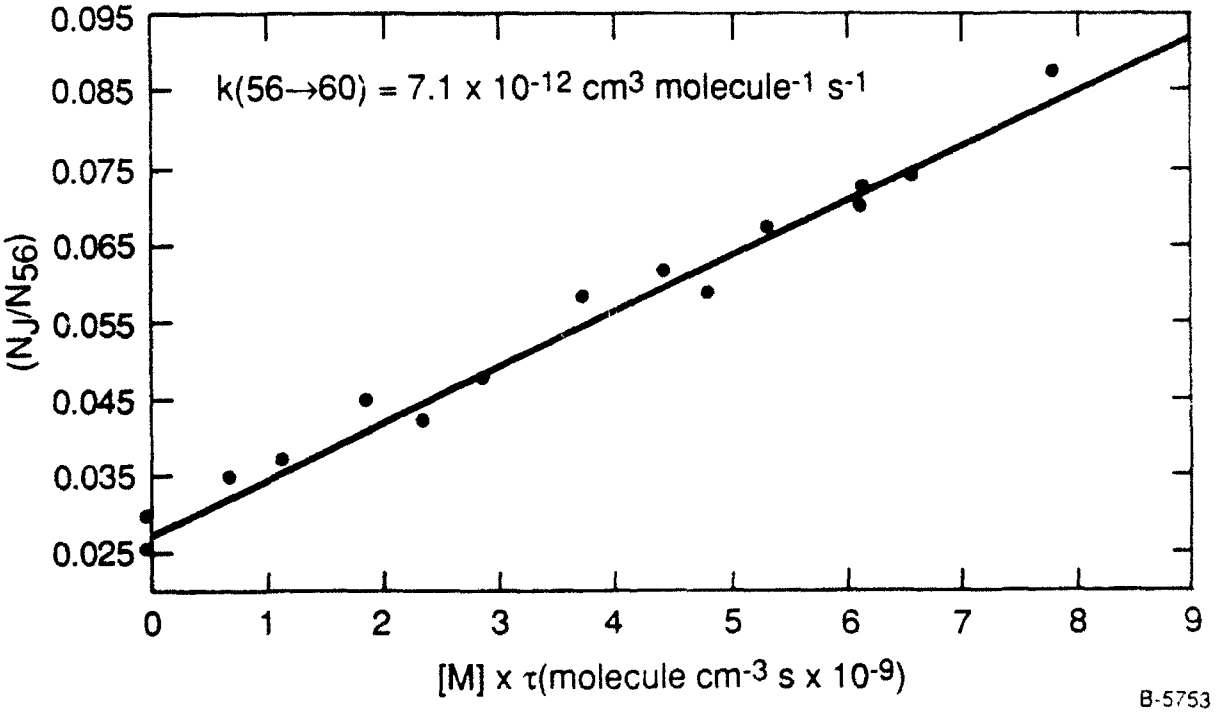


b) Stern-Volmer plot for relaxation from $J_i = 56 \rightarrow J_f = 60$

Figure 12
Stern-Volmer Plots for Two State-to-State Processes Using $O_2$ Bath Gas

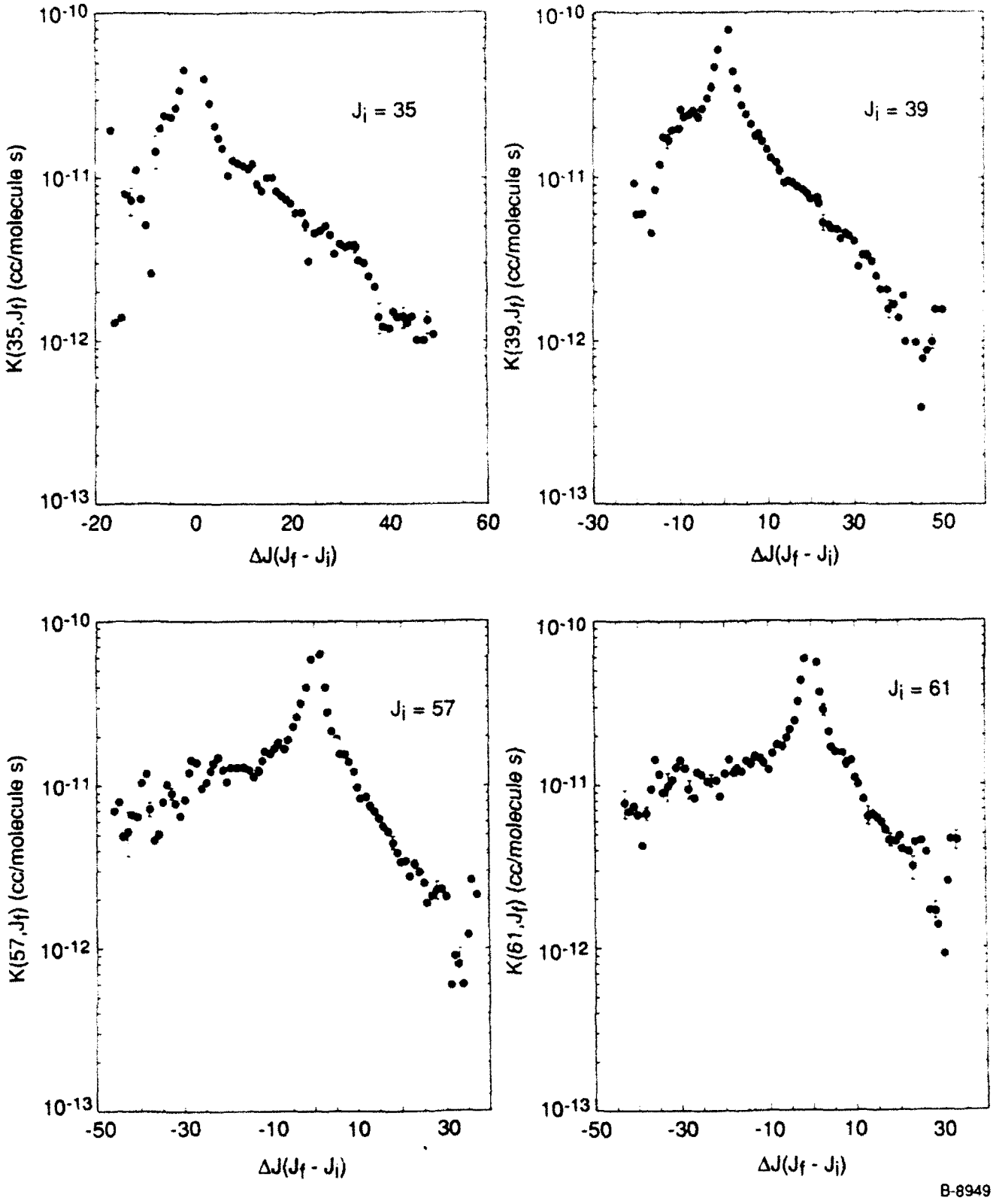


Figure 13
R-T Rate Coefficients for the ICl(B) + ICl System. Data are shown for several $J_i$.

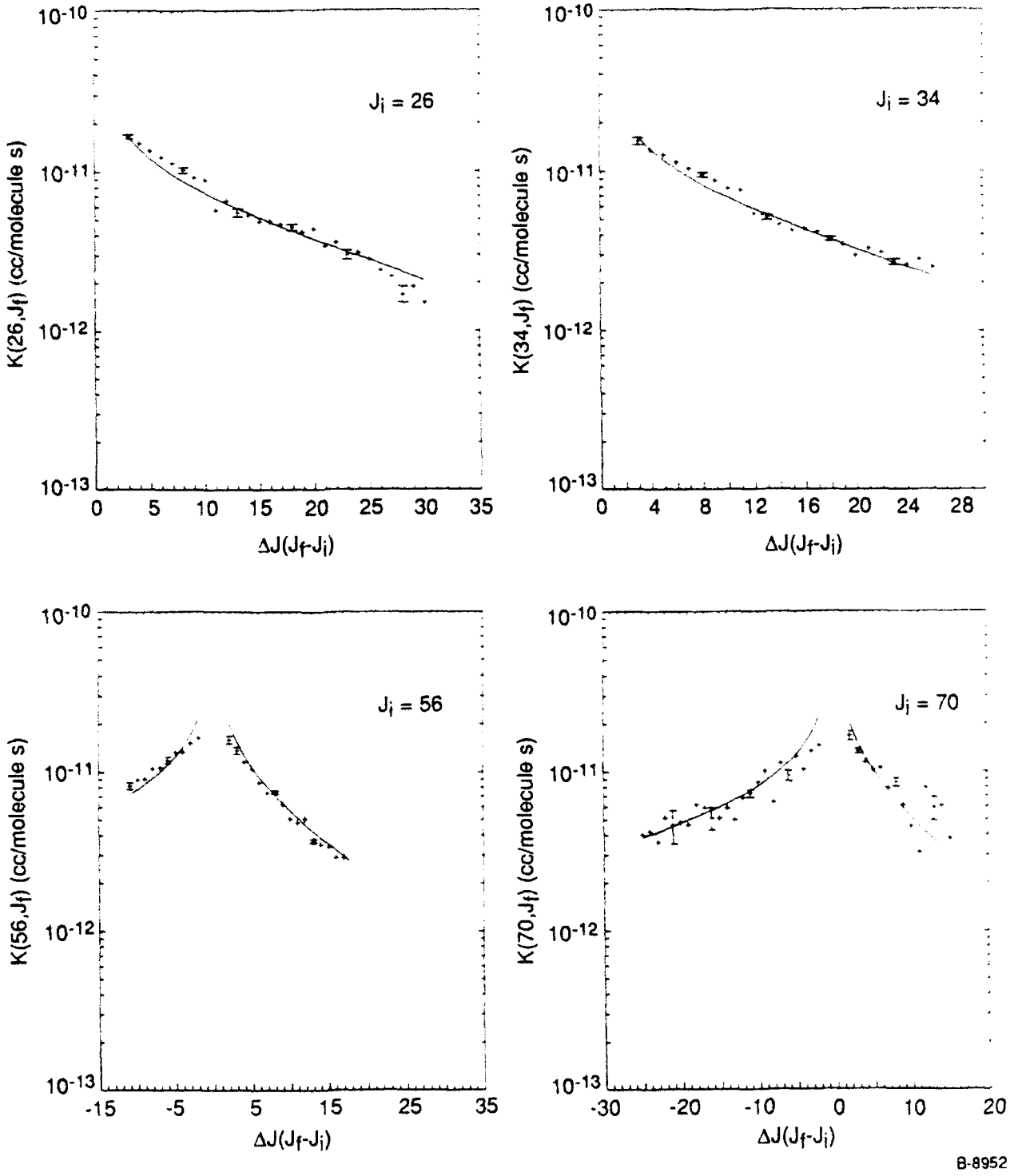


Figure 14
R-T Rate Coefficients for ICl(B) - Helium Collisions Along with "Best Fit" Coefficients Calculated Using the Infinite Order Sudden Fitting Law

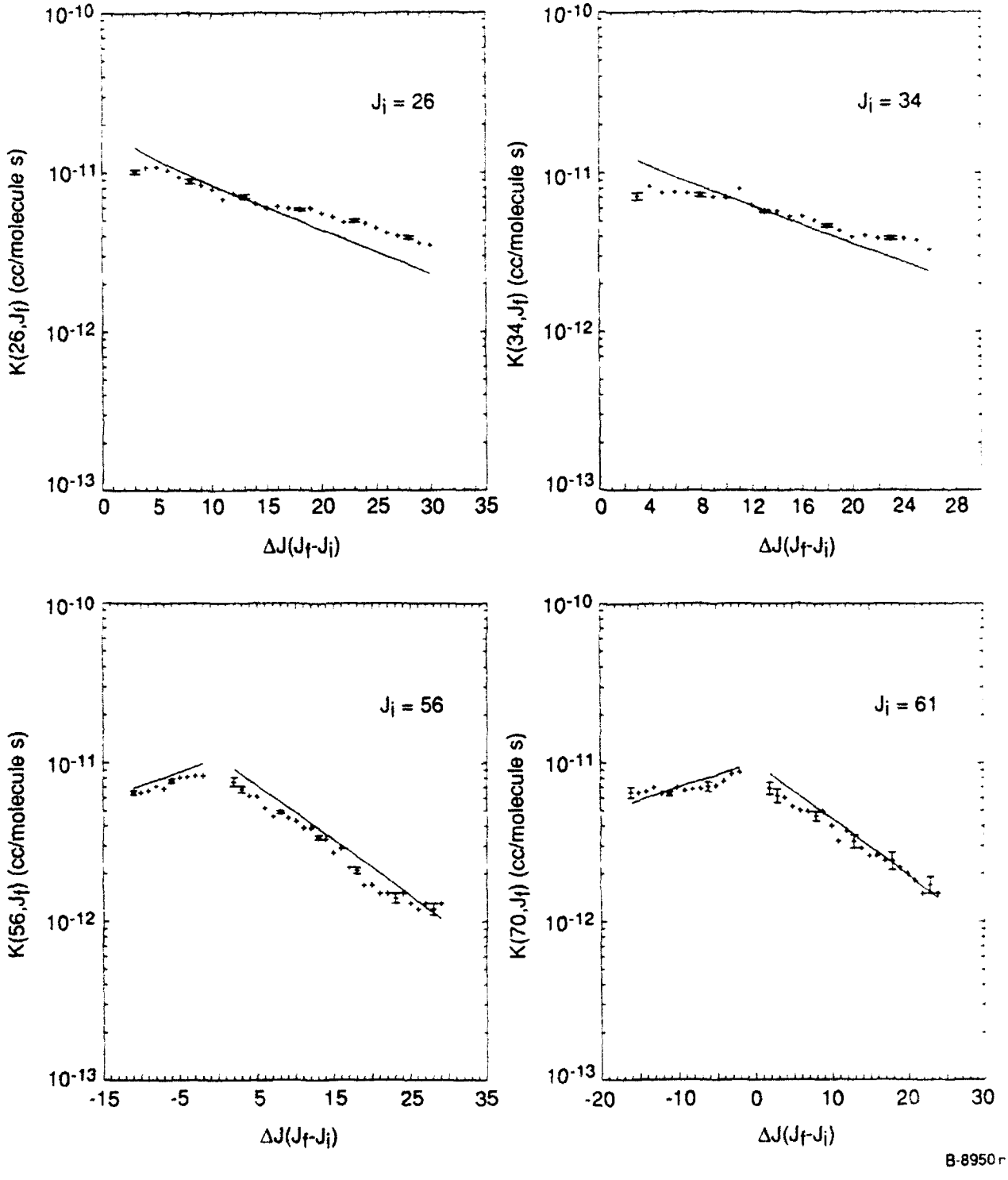


Figure 15
R-T Rate Coefficients for ICl(B) - Krypton Collisions Along with "Best Fit" Coefficients Calculated Using the Energy Corrected Sudden Fitting Law

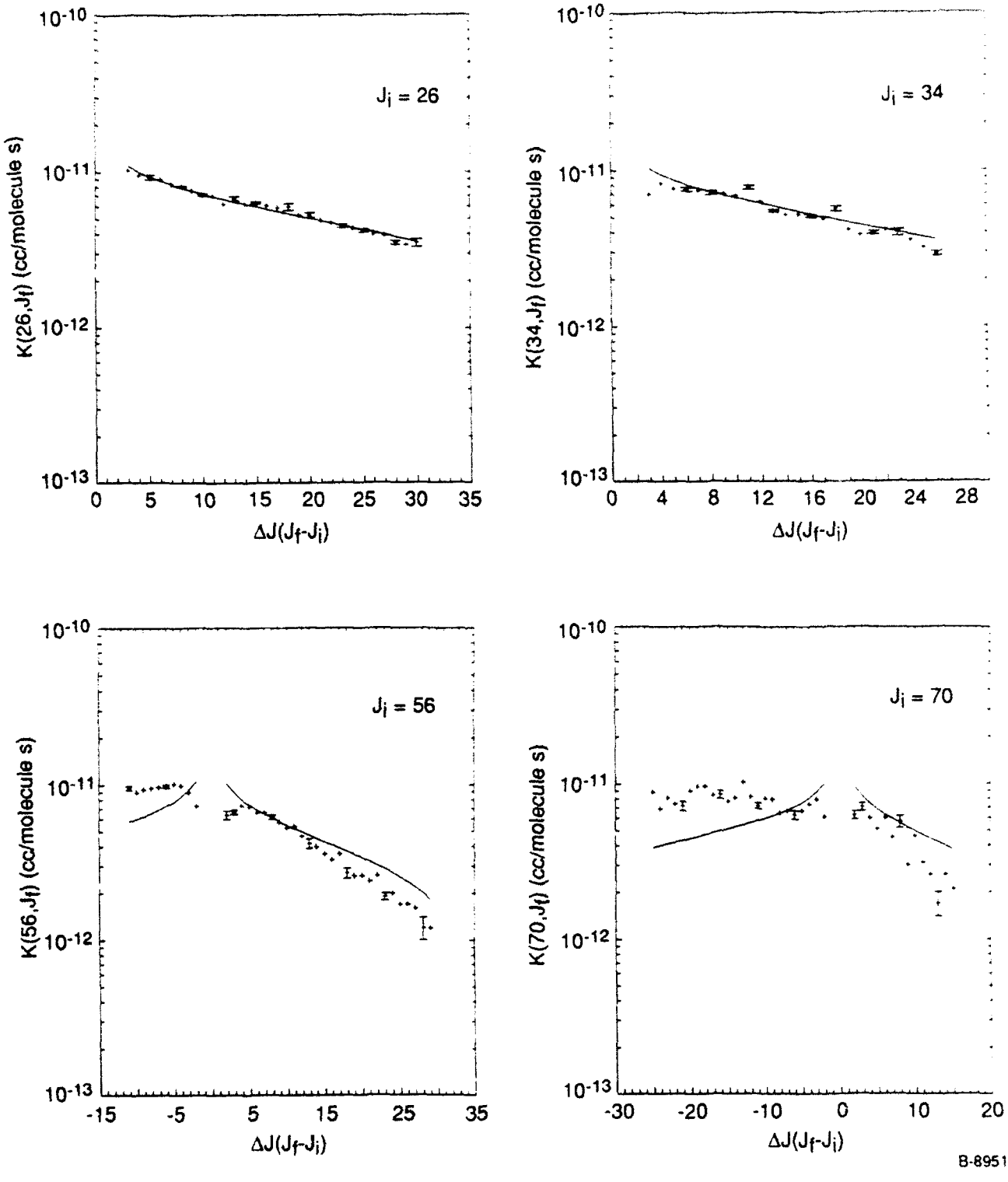


Figure 16
R-T Rate Coefficients for ICl(B) - Xenon Collisions Along With "Best Fit" Coefficients Calculated Using the Statistical Power Gap Law

Table 5. Fitting Law Results for ICL

| Bath Gas | Fitting Law | Parameters | $\chi^2$ | Δ% |
|---|---|---|---|---|
| He[a] | ECS | $a = 2.54 \times 10^{-11}$<br>$\gamma = 0.786$<br>$\ell_c = 4.85 \times 10^{-8}$ | 4.5 | 10.3 |
| | IOS | $a = 2.10 \times 10^{-11}$<br>$\gamma = 0.765$ | 5.2 | 10.9 |
| | SPG | $a = 3.19 \times 10^{-11}$<br>$\gamma = 0.892$<br>$\lambda = 75.0$ | 10.4 | 16.5 |
| | EGL | $a = 1.75 \times 10^{-13}$<br>$\theta = 1.07 \times 10^{-2}$ | 19.3 | 18.8 |
| Kr[b] | ECS | $a = 7.88 \times 10^{-11}$<br>$\gamma = 0.922$<br>$\ell_c = 1.57 \times 10^{-7}$ | 28.6 | 16.1 |
| | IOS | $a = 3.17 \times 10^{-12}$<br>$\gamma = 0.490$ | 47.5 | 28.3 |
| | SPG | $a = 3.10 \times 10^{-12}$<br>$\gamma = 0.440$<br>$\lambda = 21.48$ | 28.5 | 23.4 |
| | EGL | $a = 1.06 \times 10^{-13}$<br>$\theta = 6.20 \times 10^{-3}$ | 82.3 | 34.3 |
| Xe[c] | ECS | $a = 2.93 \times 10^{-12}$<br>$\gamma = 0.465$<br>$\ell_c = 9.7 \times 10^{-9}$ | 26.5 | 24.5 |
| | IOS | $a = 2.61 \times 10^{-10}$<br>$\gamma = 0.448$ | 26.8 | 24.9 |
| | SPG | $a = 2.26 \times 10^{-12}$<br>$\gamma = 0.331$<br>$\lambda = 14.3$ | 34.7 | 28.9 |
| | EGL | $a = 1.20 \times 10^{-13}$<br>$\theta = 5.98 \times 10^{-3}$ | 71.3 | 37.1 |

a) $J_i$=70, $J_f$=45-79; $J_i$=56, $J_f$=45-73; $J_i$=34, $J_f$=37-60; $J_i$=26, $J_f$=29-56
b) $J_i$=61, $J_f$=45-85; $J_i$=56, $J_f$=45-85; $J_i$=34, $J_f$=37-60; $J_i$=26, $J_f$=29-56
c) $J_i$=70, $J_f$=45-85; $J_i$=56, $J_f$=45-85; $J_i$=34, $J_f$=37-60; $J_i$=26, $J_f$=29-56

Table 6. Fitting Law Results for IF

| Bath Gas | Fitting Law | Parameters | $\chi^2$ | Δ% |
|---|---|---|---|---|
| He[a] | ECS | a = $3.84 \times 10^{-11}$<br>γ = 0.883<br>$\ell_c = 8.3 \times 10^{12}$ | 8.1 | 18.4 |
| | I0S | a = $4.00 \times 10^{-11}$<br>γ = 0.889 | 7.9 | 18.7 |
| | SPG | a = $3.27 \times 10^{-11}$<br>γ = 0.918<br>λ = 94.3 | 9.7 | 19.1 |
| | EGL | a = $1.35 \times 10^{-13}$<br>θ = $3.62 \times 10^{-3}$ | 11.4 | 21.1 |
| Xe[6] | ECS | a = $1.65 \times 10^{-10}$<br>γ = 1.04<br>$\ell_c = 1.0 \times 10^{-7c}$ | 12.4 | 24.5 |
| | I0S | a = $6.44 \times 10^{-12}$<br>γ = 0.644 | 36.6 | 40.9 |
| | SPG | a = $6.82 \times 10^{-12}$<br>γ = 0.509<br>λ = 11.52 | 11.5 | 23.3 |
| | EGL | a = $5.39 \times 10^{-14}$<br>θ = $1.82 \times 10^{-3}$ | 49.3 | 46.8 |

a) $J_i$=72, $J_f$=42-78; $J_i$=27, $J_f$=30-45; $J_i$=13, $J_f$16-27;
b) $J_i$=72, $J_f$=42-78; $J_i$=27, $J_f$=30-47; $J_i$=13, $J_f$16-41;
c) $\ell_c$ fixed at $1.0 \times 10^{-7}$ cm for this fit.

C.2 ICl optically-pumped laser study.

We constructed an $I_2$ laser to assure that the optical resonator was properly aligned. (The same mirrors can be used for both the $I_2$ and the ICl lasers.) Strong laser action on the $I_2$ system was readily observed as shown in Figure 17. Excitation was on the (14, 0) band. The excitation spectrum was obtained by monitoring the $I_2$ laser output as a function of dye laser excitation wavelength.

In Figure 18 we show a similar scan using ICl as the active medium. While these data should be considered preliminary there are clear differences between the two spectra. In order to minize contamination caused by $I_2$, we tried several ICl sources. For example, we subjected a sample of ICl to numerous freeze/thaw cycles. We also used $ICl_3$ crystals as the source. This is the same approach that we use in the ring laser ICl RET studies.

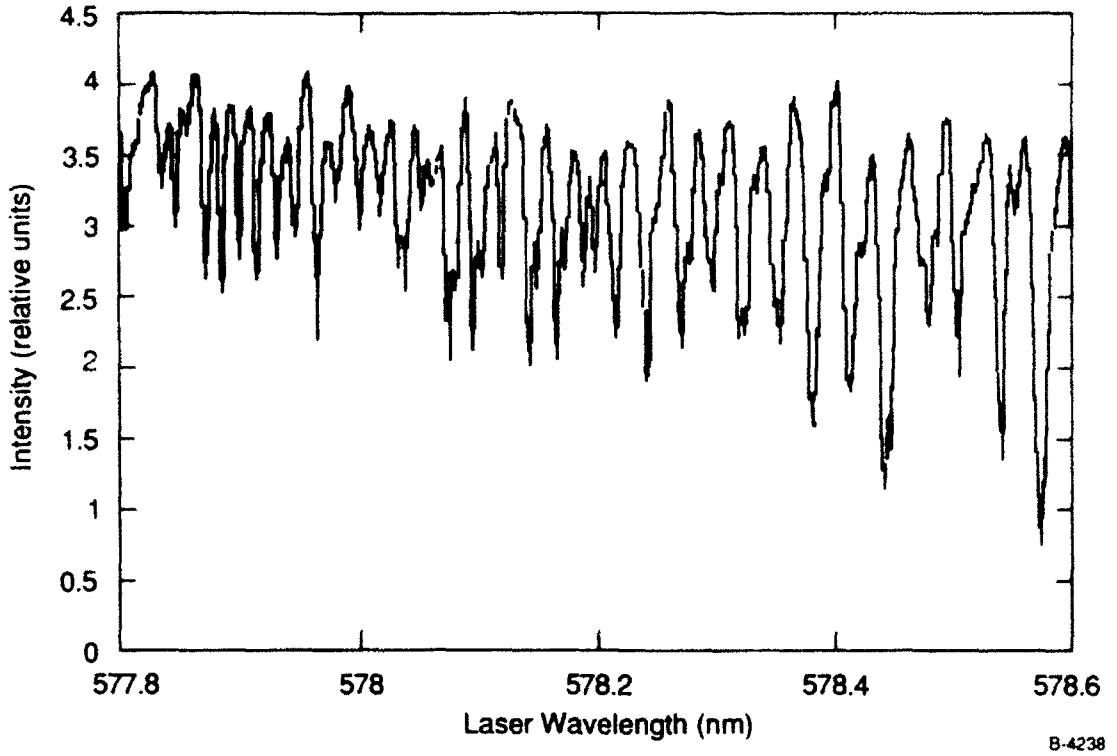


Figure 17
Laser Excitation Spectrum Using $I_2$ as the Active Medium.

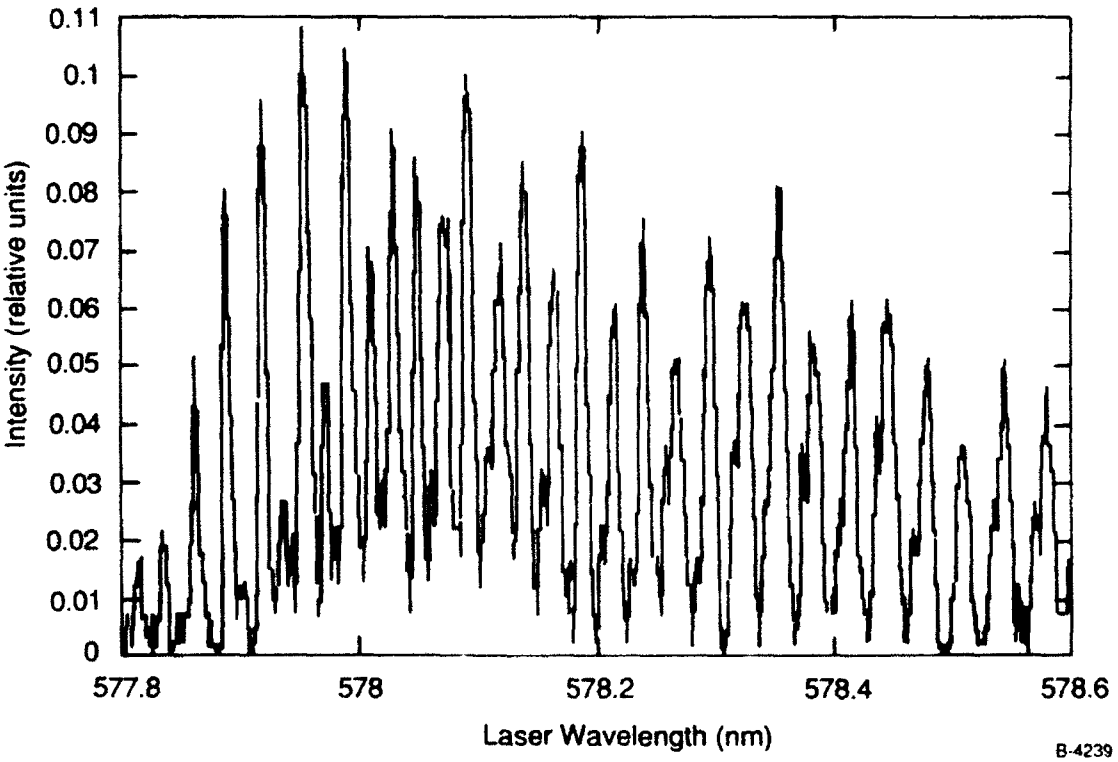


Figure 18
Laser Excitation Spectrum Using ICl as the Active Medium.

Although this reduced the $I_2$ contamination strong $I_2$ LIF signals were still observed. Part of the problem is the rather wide bandwidth of the pulsed dye laser (0.1 $cm^{-1}$). Consequently, it may be difficult to excited isolated lines of ICl in the presence of even trace amounts of $I_2$ and weak ICl lasing could be unobservable in the presence of $I_2$ laser. In contrast, we have already demonstrated that the ring dye laser is capable of exciting a single ICl absorption feature. Thus the ring dye laser might serve as an attractive excitation source for an ICl laser. Due to programmatic desires of the Air Force, we focused most of our attention for the remainder of the contract on overtone-pumped lasers, and were unable to attempt the CW optically-pumped laser experiments on ICl. We feel that this would be a fruitful set of experiments to try.

Nevertheless, our preliminary data indicate that we may have succeeded in demonstrating a pulsed ICl (B→X) laser. The key point is that lasing is observed at excitation wavelengths distinct from those for $I_2$.

C.3 $O_4$ dimole laser support.

In an effort to examine further the emission spectra reported by Yoshida et al.[20] we have used our spectral simulation code to predict the $Cl_2$(B→X) emission system for a variety of conditions. In Figures 19 through 23 we present some of these results. The two parameters that we varied were: a) vibrational distribution the B state and b) the resolution element to mimic the instrumental response of the monochromator used by Yoshida.[20] These synthetic spectra show that the observed emission is a sensitive function of both the instrumental bandwidth and the initial vibrational distribution. It is of interest and perhaps significant that the spectra observed by Yoshida is qualitatively similar to our $Cl_2$(B→X) spectrum. While this certainly does not confirm the emission originating from $Cl_2$, is it suggestive that the chemiluminescence may be from species other than $O_4^*$

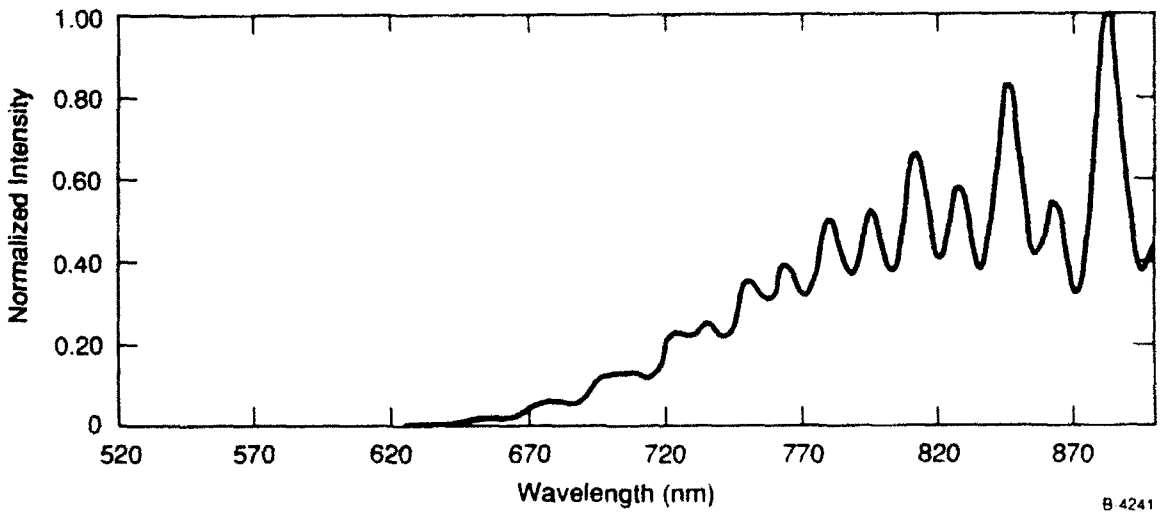


Figure 19
Synthetic $Cl_2$ (B→X) spectrum. 10 nm Resolution; $T_R = T_{vib} = 300$ K

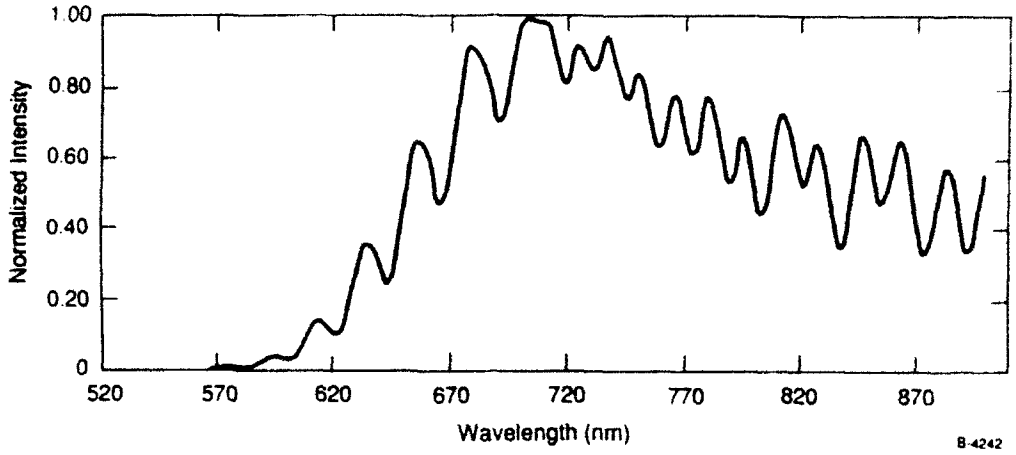


Figure 20
Synthetic $Cl_2$ (B→X) Spectrum. 10 nm resolution; relative vibrational distribution as follows: $v'_0 = 1$, $v'_1 = 1$, $v'_2 = 1$, $v'_3 = 1$, $v'_4 = 1$

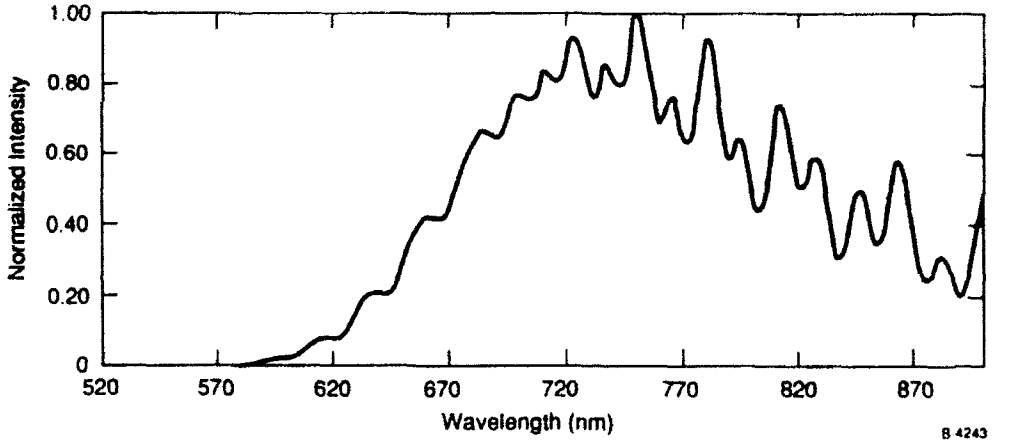


Figure 21
Synthetic $Cl_2$ (B→X) Spectrum. 10 nm resolution; relative vibrational distribution as follows: $v'_0 = 0.33$, $v'_1 = 0.66$, $v'_2 = 1.0$, $v'_3 = 0.66$, $v'_4 = 0.33$

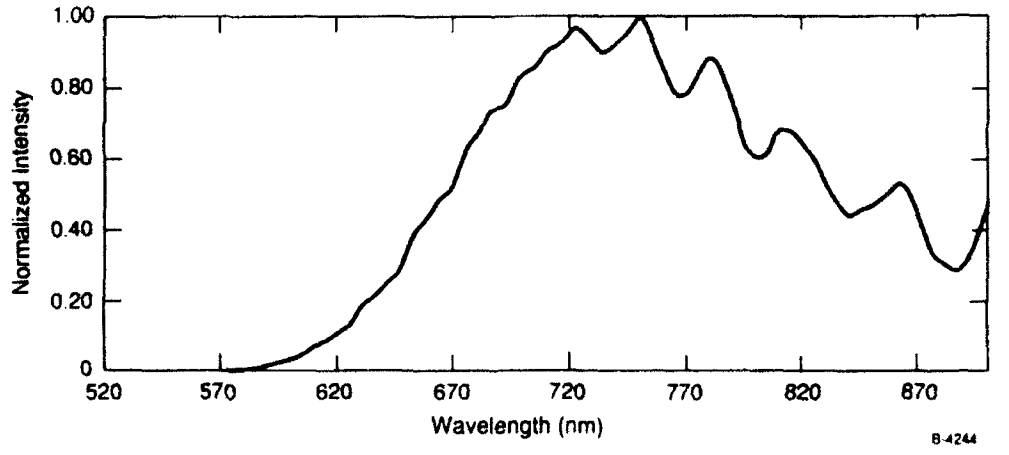


Figure 22
Synthetic $Cl_2$ (B→X) Spectrum. 15 nm resolution; vibrational distributions same as for Figure 21

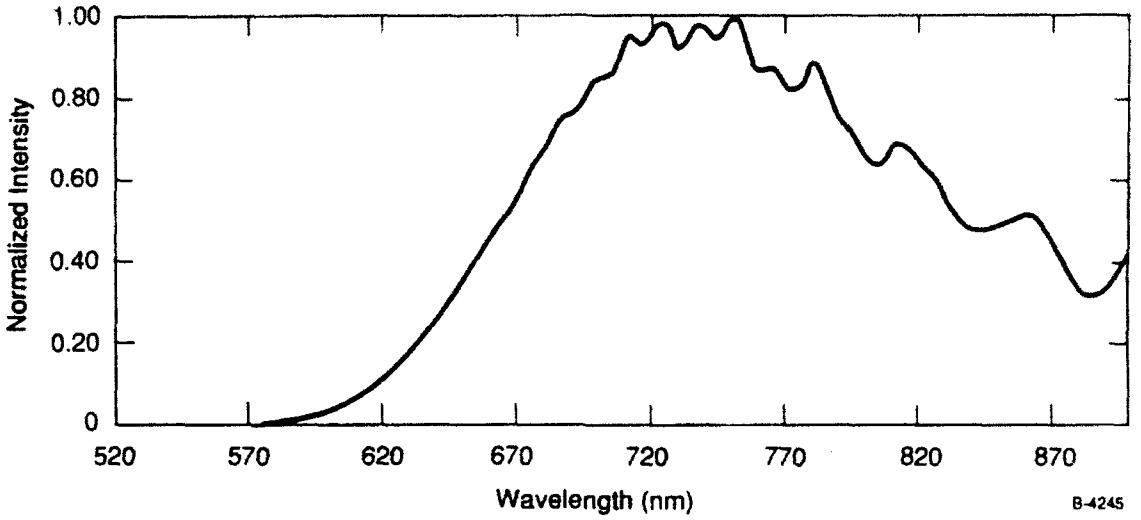


Figure 23
Synthetic $Cl_2$ (B→X) Spectrum. 20 nm resolution;
vibrational distributions same as for Figure 21

C.4 Vibrational relaxation in IF(X).

In Figure 24 we present data showing the decay of IF(X,v=9) in the fast flow reactor. We have plotted $\ln[IF(X,v=9)]_{t=0}/\ln[IF(X,v=9)]_t$ as a function of the reaction time. These data were for a 2/1 mix of helium and argon at a concentration of 0.65 Torr. From these data we estimate that the V-T relaxation rate is $\sim 6 \times 10^{-14}$ $cm^3$ $molecule^{-1}$ $s^{-1}$. These preliminary estimates indicate that relaxation is extremely slow. Thus, IF(X,v) may be a robust energy reservoir.

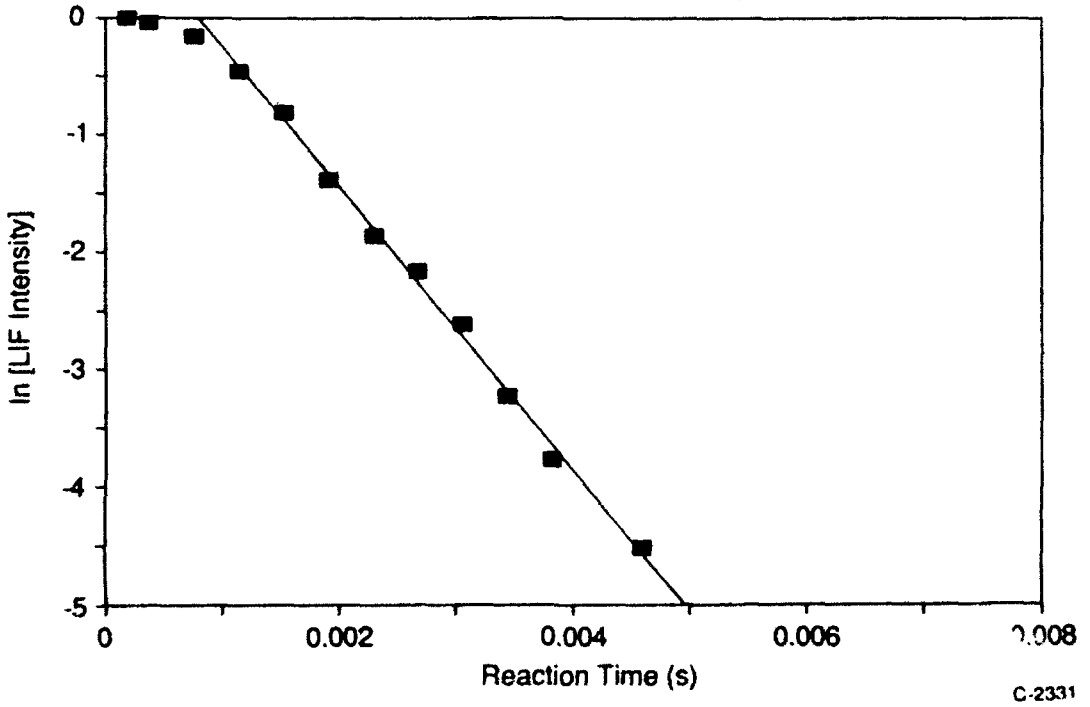


Figure 24
Decay of IF(X,v=9) in Presence of 2/1 Helium/Argon Mix at a Pressure of 0.65 Torr.

C.5 Optically-pumped overtone HF laser.

In Figure 25 we present an absorption spectrum for several rotational lines in the HF(2,0) overtone band. These data were obtained by monitoring the Raman shifted dye laser output that was transmitted through the cell that contained HF gas. Also shown in Figure 25 are data obtained by increasing the pump power of the Raman shifted dye laser. The strong emission features are due to amplified spontaneous emission (ASE). These data were obtained in the 7.5 cm cell that contained 50 Torr of HF and 670 Torr of helium. The features appear sharper than the absorption lines because there is a threshold power level for ASE.

The pump intensity threshold for the ASE was quite low as indicated in Figure 26. These data obtained in the 7.5 cm cell containing 50 Torr of HF indicate a threshold energy of less than 100 $\mu$J. Since this was for a mirrorless cell with no feedback, we estimate that in a cavity, less than 10 $\mu$J of pump excitation will be required.

We found that the ASE output power was independent of added helium bath gas as indicated in Figure 27. This is an encouraging result since the addition of a collisional bath gas will broaden the overtone absorption line. This may enhance the coupling of pump lasers into the laser media.

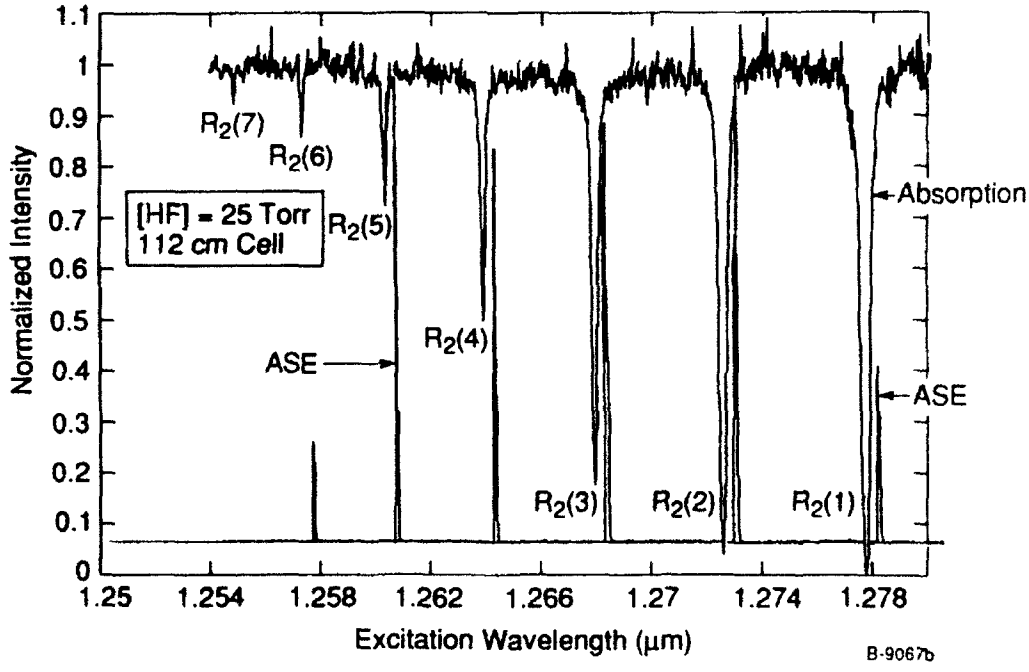


Figure 25
Absorption Spectra and Corresponding ASE Spectra for Overtone-pumping Several R-branch Lines on the HF(2,0) Overtone Band. The top spectrum shows absorption of the dye laser and the bottom trace shows the ASE excitation spectrum. The two spectra have been offset slightly for clarity.

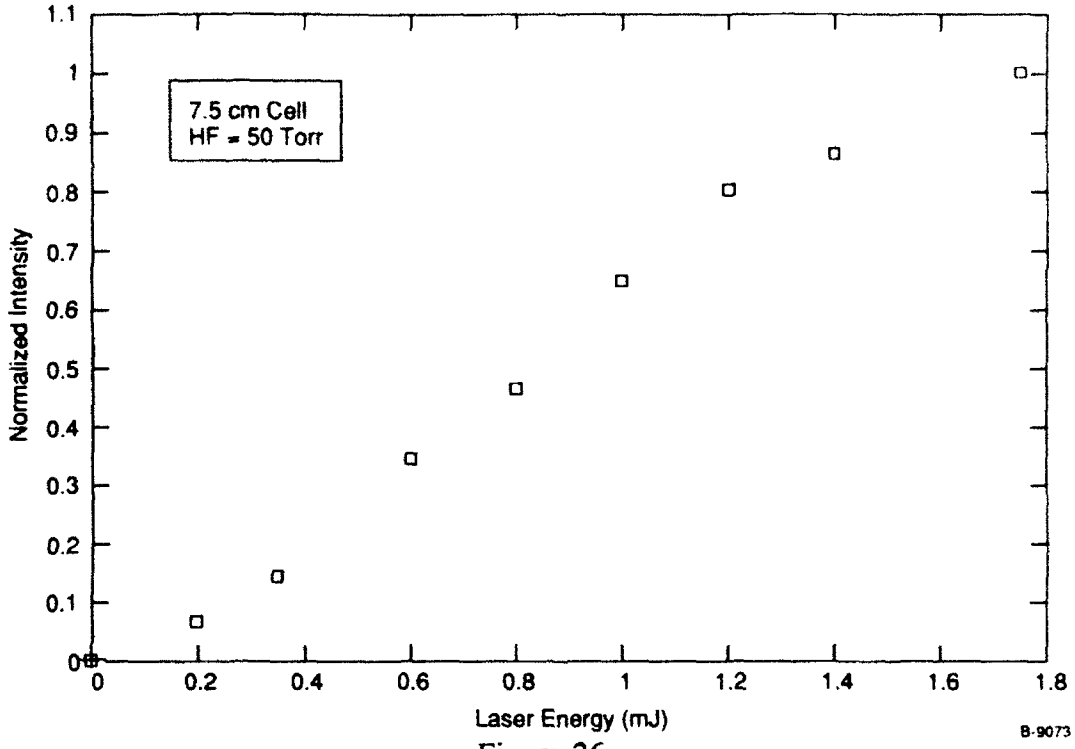


Figure 26

ASE Output as a Function of Pump Energy Incident on the Cell. The R(3) line of v=2 in HF was excited for these data.

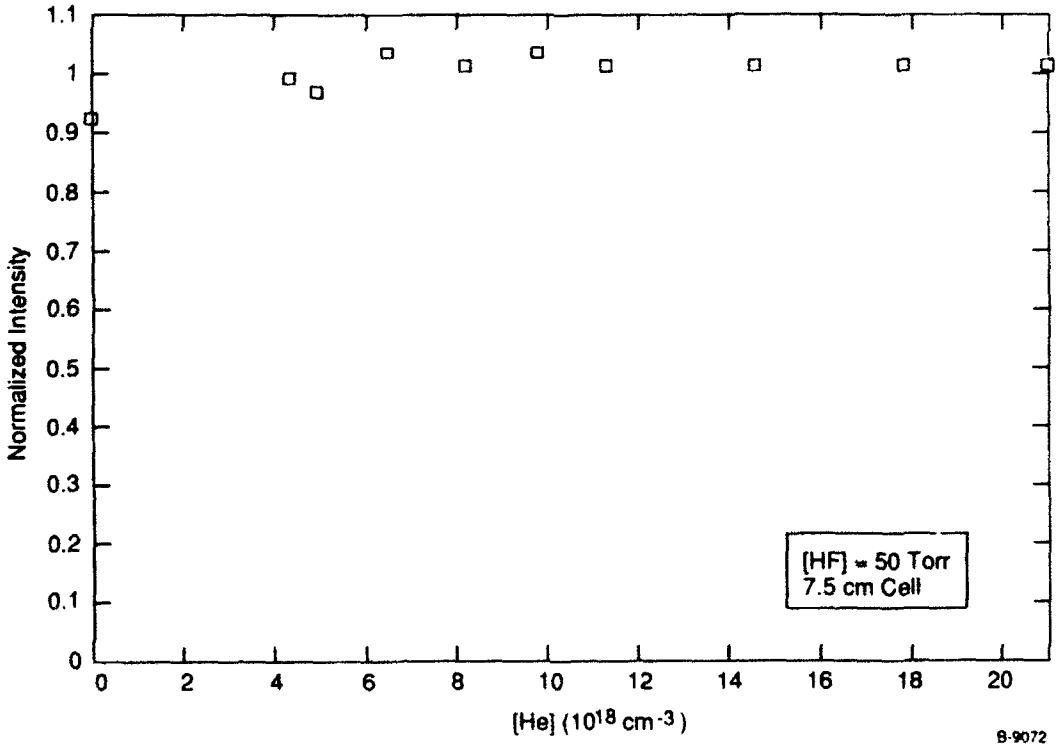


Figure 27

Output of HF ASE as a Function of Added Helium. The R(3) line in v=2 was pumped.

We also found that the ASE was quite insensitive to the HF concentration. In Figure 28 we present data that were obtained pumping the R(3) line with 2 mJ of excitation incident upon the cell. There is an initial rise as the concentration increased from 0 to about 100 Torr. As more HF is added collision deactivation of the optically pumped level begins to exceed the excitation rate and the output energy drops. These data however indicate that the HF overtone-pumped laser is quite immune to self quenching.

We also performed some experiments in which the output of the ASE was spectrally resolved. These experiments provide important insights into the energy pathways and energy transfer within the excited state manifolds. For these experiments we placed a 0.3m monochromator in front of the InAs detector. Some typical data are presented in Figure 29.

For clarity, both the observed spectra and the associated energy levels are presented in Figure 29. These data illustrate an important feature of the overtone-pumped HF laser. We pumped the P(2) line of the (3,0) band near 875 nm. We observe ASE from both rotational and vibrational levels distinct from the level initially excited by the dye laser. Indeed, rotational relaxation in the initially pumped v=3 level is evident. From a practical perspective our observation of ASE from both the (3,2) and (2,1) bands indicates cascading laser emission. Thus one may be able to recover a large fraction of the initial photons that were absorbed by the medium. These experiments should be repeated using an optical resonator. Nevertheless, these initial measurements are very encouraging.

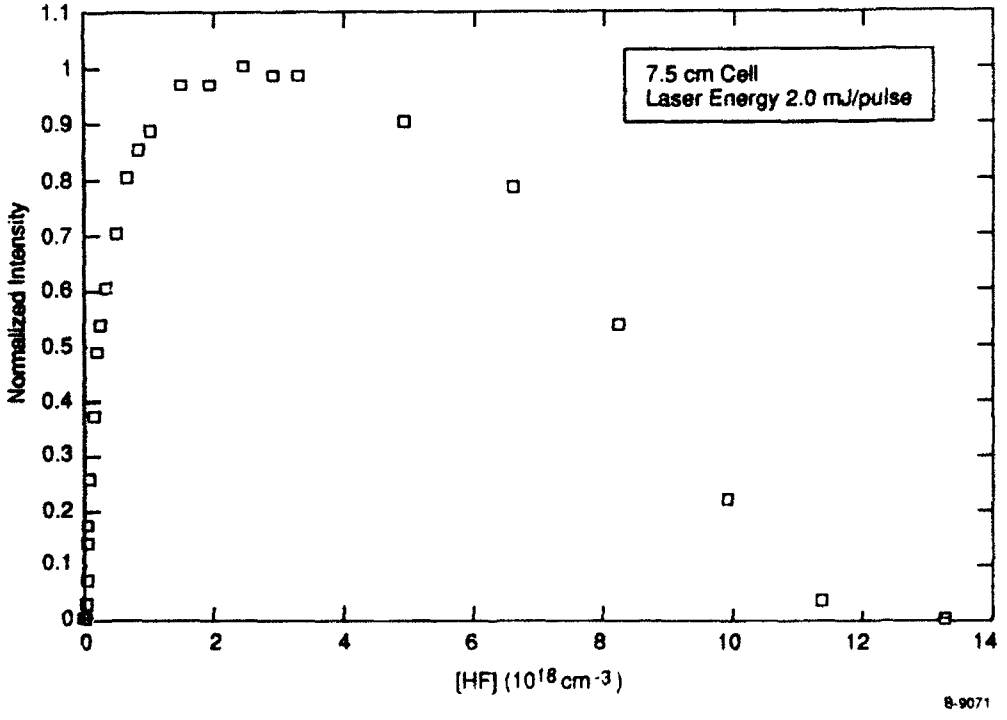


Figure 28
ASE Signal Strength as a Function of Added HF.
The R(3) line in the (2,0) band was excited for these data.

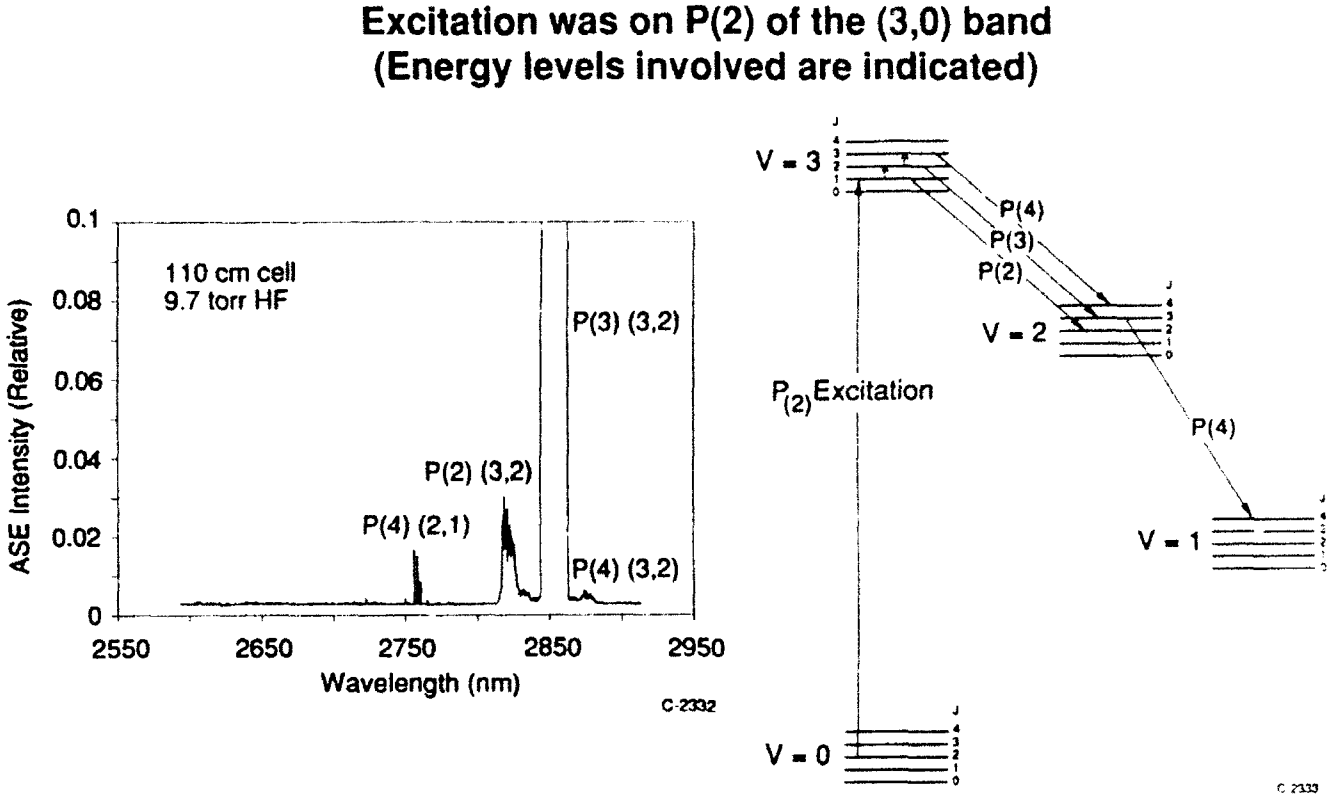


Figure 29
Spectrally Resolved HF ASE Output Following Excitation of v=3.

An eventual gas phase overtone-pumped laser might be excited by a tunable diode laser. In an initial attempt to demonstrate the potential of this approach, we used a low power (2mW) heterostructure near infrared diode laser to probe a cell of HF. Strong absorption was observed when the dye laser was tuned to the P(3) line of the (2,0) band near 1.26 microns. In Figure 30 we show data using the 7.5 cm cell filled with 9 Torr of HF. The absorption approaches 90% as expected from the strong overtone absorption cross sections. The potential for using a high power diode laser to produce an optically-pumped HF laser is apparent, and we will pursue this approach in our follow on effort.

Summary

We have described the results of a program that has examined energy transfer in several systems. In addition, we have discussed applications to several Air Force programs. In particular we focussed our attention in year three on near-IR lasers, an emerging Air Force need. We will explore these concepts further in our follow-on program.

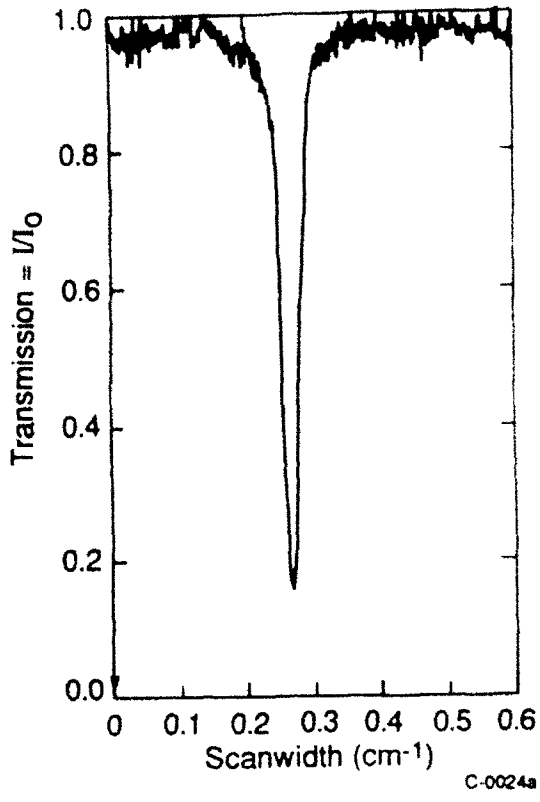


Figure 30
Absorption Spectrum of HF P(3) on the (2,0) band.
The 7.5 cm cell contained 9 Torr of HF.

References

1. Davis, S.J., and Holtzclaw, K.W., "Rotational Energy Transfer in Excited States of Halogen Molecules, I. Transfer from v'=6, J'=72 in IF $B^3\Pi(0+)$, J. Chem. Phys., 92, 1661 (1990).

2. Wolf, P.J., and Davis, S.J., "Collisional Dynamics of the IF $B^3\Pi(0+)$ State. II. Electronic Quenching at Low Pressures", J. Chem. Phys., 83, 91 (1985).

3. Wolf, P.J., and Davis, S.J., "Collisional Dynamics of the IF $B^3\Pi(0+)$ State, III. Vibrational and Rotational Energy Transfer", J. Chem. Phys., 87, 3492 (1987).

4. Girard, B., Billy, N., Gouedard, G., and Vigue, J., J. Chem. Phys., 88, 2342 (1988).

5. Clyne, M.A.A., and McDermid, I.S., "Quantum-resolved Dynamics of Excited States, Part 4. Radiative and Predissociative Lifetimes of IF $B^3\Pi(0+)$.", J. Chem. Soc., Far. Trans. II, 4, 1644 (1978).

6. Kitimura, M., Kondow, T., Kuchitsu, K., Munakata, T., and Kasuya, T., "Fluorescence Lifetimes and Spontaneous Predissociation of $I^{35}Cl$ (B0+, v'=1 and 2) as studied by Laser excited fluorescence", J. Chem. Phys., 82, 4986 (1985).

7. Clyne, M.A.A. and McDermid, I.S., $B^3\Pi(0+)$ States of IF, ICl, and IBr Part 1. Calculation of the RKR Turning Points and Franck-Condon Factors for the B-X Systems", J. Chem. Soc. Faraday Trans. II, 73, 1094 (1977).

8. Gordon, R.D. and Innes, K.K., "Predissociations in the $B^3\Pi0+$ State of $I^{35}Cl$ and $I^{37}Cl$", J. Chem. Phys., 71, 2824 (1979).

9. Trickl, T. and Wanner, J., "High-Resolution, Laser-Induced Fluorescence Spectroscopy of Nascent IF: Determination of X- and B-State Molecular Constants", J. Mol. Spect., 104, 174 (1984).

10. Brand, J.C.D. and Hoy, A.R., "High Vibrational Levels of the X State of ICl, and the Electronic-Coriolis Coupling of the X and A States", J. Mol. Spect., 114, 197 (1985).

11. Brunner, T.A. and Pritchard D., "Fitting Laws for Rotationally Inelastic Collisions", Dynamics of the Excited State, Ed. K.P. Lawley, pp. 589-641, John Wiley & Sons. Ltd., New York, 1982.

12. Steinfeld, J.I., and Ruttenberg, P., "Scaling Laws for Inelastic Collision Processes in Diatomic Halogens", JILA Information Center Report No. 23, (1983).

13. Brunner, T.A., Smith, N., Karp, A.W., and Pritchard, D., "Rotational Energy Transfer in $Na_2$ ($A^2\Sigma$) Colliding with Xe, Kr, Ar, Ne, He, $H_2$, $CH_4$, and $N_2$: Experiment and Fitting Laws", J. Chem. Phys., 74, 3324 (1980).

14. Polanyi, J.E. and Woodall K.B., "Mechanisms of Rotational Relaxation", J. Chem. Phys., 56, 1563 (1972).

15. Brunner, T.A., Driver, R.D., Smith N., and Pritchard, D., "Simple Scaling Law for Rotational-Energy Transfer in $Na_2$*-Xe Collisions", Phys. Rev. Lett., 41, 856 (1978).

16. Dexheimer, S.L., Durand, M., Brunner, T.A., and Pritchard D.E., "Dynamical Constraints on the Transfer of Angular Momentum in Rotationally Inelastic Collisions of I2(B3$\pi$(0+) with He and Xe", J. Chem. Phys., 76, 4996 (1982).

17. DePristo, A.E., Augustin, S.D., Ramaswamy, R., and Rabitz, H., "Quantum Number and Energy Scaling for Nonreactive Collisions", J. Chem. Phys., 71, 850 (1979).

18. Scott, T.P., Smith, N., and Pritchard D.E., "Application of Fitting Laws to Rotationally Inelastic Rate Constants: Li2*(a1sigma) + Ne, Ar, Xe", J. Chem. Phys., 80, 4841 (1984).

19. Bevington, P.R., Data Reduction and Error Analysis for the Physical Sciences, McGraw-Hill, New York, 1969.

20. Yoshida, S., Shimizu, K., Sawano, T., Tokuda, T., and Fujioka, T., Apply. Phys. Lett. 54, 24 (1989).

21. Davis, S.J. and Woodward, A.M., "Excitation of IFB($^3\Pi O^+$) by Metastable $O_2$. 1. Studies Involving IF(X,v)". J. Phys. Chem. 95, 2429 (1991).

22. Trickl, T. and Wanner, J. J. Chem. Phys. 78 6091 (1983).

# Appendix

## Summary of Rate Coefficients Measured for ICl Collisions with Several Bath Gases

Initially populated levels ($J_i$) are indicated. Rate coefficients (k ($J_i$, $J_f$)) and standard deviations ($\sigma$) determined from Stern-Volmer plots are tabulated.

Table A-1. Rate Coefficeints for ICl + He Collisions

| ICl + He ($J_i$ = 26, $v_i'$=1) | | | ICl + He ($J_i$ = 26, $v_i'$=1) | | |
|---|---|---|---|---|---|
| | ($10^{-12}$ cm$^3$ molecule$^{-1}$ s$^{-1}$) | | | ($10^{-12}$ cm$^3$ molecule$^{-1}$ s$^{-1}$) | |
| $J_f$ | $k(J_i,J_f)$ | $\sigma$ | $J_f$ | $k(J_i,J_f)$ | $\sigma$ |
| 20 | 12.6 | 1.3 | 58 | 1.2 | 0.2 |
| 21 | 11.8 | 0.5 | 59 | 0.8 | 0.2 |
| 22 | 14.5 | 1.3 | 60 | 1.0 | 0.2 |
| 23 | 14.9 | 1.0 | 61 | 0.8 | 0.1 |
| 24 | 15.0 | 1.7 | 62 | 0.7 | 0.1 |
| 25 | 15.7 | 1.0 | 63 | 0.9 | 0.1 |
| 26 | 0.0 | 0.0 | 64 | 0.9 | 0.1 |
| 27 | 11.3 | 1.5 | 65 | 0.7 | 0.1 |
| 28 | 20.2 | 1.4 | 66 | 0.7 | 0.1 |
| 29 | 16.6 | 0.5 | | | |
| 30 | 15.1 | 0.7 | | | |
| 31 | 13.6 | 0.7 | | | |
| 32 | 12.3 | 0.8 | | | |
| 33 | 11.4 | 0.5 | | | |
| 34 | 10.3 | 0.4 | | | |
| 35 | 9.3 | 0.4 | | | |
| 36 | 8.9 | 0.5 | | | |
| 37 | 5.8 | 0.4 | | | |
| 38 | 6.6 | 0.3 | | | |
| 39 | 5.6 | 0.3 | | | |
| 40 | 5.4 | 0.3 | | | |
| 41 | 4.9 | 0.4 | | | |
| 42 | 4.9 | 0.2 | | | |
| 43 | 4.7 | 0.2 | | | |
| 44 | 4.5 | 0.2 | | | |
| 45 | 4.2 | 0.4 | | | |
| 46 | 4.4 | 0.3 | | | |
| 47 | 3.4 | 0.1 | | | |
| 48 | 3.6 | 0.2 | | | |
| 49 | 3.0 | 0.2 | | | |
| 50 | 3.1 | 0.1 | | | |
| 51 | 2.8 | 0.1 | | | |
| 52 | 2.4 | 0.1 | | | |
| 53 | 2.2 | 0.1 | | | |
| 54 | 1.7 | 0.2 | | | |
| 55 | 1.9 | 0.2 | | | |
| 56 | 1.5 | 0.1 | | | |
| 57 | 1.6 | 0.1 | | | |

Table A-1. Rate Coefficeints for ICl + He Collisions (Continued)

| ICl + He ($J_i$ = 34, $v_i$=1) | | | ICl + He ($J_i$ = 34, $v_i$=1) | | |
|---|---|---|---|---|---|
| | ($10^{-12}$ cm$^3$ molecule$^{-1}$ s$^{-1}$) | | | ($10^{-12}$ cm$^3$ molecule$^{-1}$ s$^{-1}$) | |
| $J_f$ | $k(J_i,J_f)$ | $\sigma$ | $J_f$ | $k(J_i,J_f)$ | $\sigma$ |
| 27 | 18.4 | 0.6 | 68 | 0.8 | 0.1 |
| 28 | 13.7 | 0.8 | 69 | 0.8 | 0.1 |
| 29 | 13.7 | 0.7 | 70 | 0.7 | 0.1 |
| 30 | 15.7 | 0.6 | 71 | 0.7 | 0.1 |
| 31 | 16.0 | 0.9 | 72 | 0.6 | 0.1 |
| 32 | 17.5 | 0.8 | 73 | 0.7 | 0.1 |
| 33 | 12.5 | 1.0 | 74 | 0.3 | 0.1 |
| 34 | 0.0 | 0.0 | | | |
| 35 | 17.9 | 0.9 | | | |
| 36 | 12.8 | 1.1 | | | |
| 37 | 15.4 | 0.7 | | | |
| 38 | 13.6 | 0.6 | | | |
| 39 | 12.6 | 0.6 | | | |
| 40 | 11.5 | 0.4 | | | |
| 41 | 10.4 | 0.5 | | | |
| 42 | 9.6 | 0.3 | | | |
| 43 | 8.8 | 0.3 | | | |
| 44 | 7.9 | 0.2 | | | |
| 45 | 7.7 | 0.3 | | | |
| 46 | 5.5 | 0.2 | | | |
| 47 | 5.2 | 0.2 | | | |
| 48 | 4.7 | 0.2 | | | |
| 49 | 4.3 | 0.1 | | | |
| 50 | 4.4 | 0.1 | | | |
| 51 | 4.2 | 0.1 | | | |
| 52 | 3.8 | 0.1 | | | |
| 53 | 3.5 | 0.1 | | | |
| 54 | 3.0 | 0.2 | | | |
| 55 | 3.3 | 0.1 | | | |
| 56 | 3.1 | 0.1 | | | |
| 57 | 2.7 | 0.1 | | | |
| 58 | 2.6 | 0.2 | | | |
| 59 | 2.8 | 0.2 | | | |
| 60 | 2.5 | 0.1 | | | |
| 61 | 1.8 | 0.1 | | | |
| 62 | 1.9 | 0.2 | | | |
| 63 | 1.5 | 0.1 | | | |
| 64 | 1.3 | 0.1 | | | |
| 65 | 1.3 | 0.1 | | | |
| 66 | 1.2 | 0.1 | | | |
| 67 | 0.9 | 0.1 | | | |

Table A-1. Rate Coefficeints for ICl + He Collisions (Continued)

| ICl + He ($J_i$ = 56, $v'_i$ = 1) | | | ICl + He ($J_i$ = 56, $v'_i$ = 1) | | |
|---|---|---|---|---|---|
| | ($10^{-12}$ cm$^3$ molecule$^{-1}$ s$^{-1}$) | | | ($10^{-12}$ cm$^3$ molecule$^{-1}$ s$^{-1}$) | |
| $J_f$ | $k(J_i,J_f)$ | $\sigma$ | $J_f$ | $k(J_i,J_f)$ | $\sigma$ |
| 22 | 3.1 | (0.3) | 62 | | (0.3) |
| 23 | 1.8 | (0.3) | 63 | | (0.3) |
| 24 | 2.2 | (0.4) | 64 | | (0.2) |
| 25 | 1.7 | (0.3) | 65 | 6.3 | (0.1) |
| 26 | 2.6 | (0.3) | 66 | 5.1 | (0.2) |
| 27 | 3.6 | (0.4) | 67 | 4.8 | (0.3) |
| 28 | 2.1 | (0.6) | 68 | 5.1 | (0.2) |
| 29 | 4.7 | (0.3) | 69 | 3.7 | (0.1) |
| 30 | 4.2 | (0.3) | 70 | 3.5 | (0.2) |
| 31 | 4.0 | (0.5) | 71 | 3.4 | (0.2) |
| 32 | 4.3 | (0.3) | 72 | 2.9 | (0.2) |
| 33 | 4.3 | (0.3) | 73 | 2.9 | (0.2) |
| 34 | 5.0 | (0.2) | 74 | 3.7 | (0.2) |
| 35 | 4.8 | (0.3) | 75 | 2.5 | (0.2) |
| 36 | 5.2 | (0.4) | 76 | 1.9 | (0.1) |
| 37 | 5.4 | (0.5) | 77 | 2.2 | (0.1) |
| 38 | 5.6 | (0.3) | 78 | 1.5 | (0.1) |
| 39 | 5.8 | (0.5) | 79 | 1.9 | (0.2) |
| 40 | 5.8 | (0.3) | 80 | 1.5 | (0.2) |
| 41 | 5.7 | (0.3) | 81 | 0.7 | (0.1) |
| 42 | 5.8 | (0.2) | 82 | 1.2 | (0.1) |
| 43 | 6.2 | (0.3) | 83 | 1.4 | (0.1) |
| 44 | 6.3 | (0.4) | 84 | 1.0 | (0.1) |
| 45 | 8.2 | (0.4) | 85 | 1.0 | (0.2) |
| 46 | 8.9 | (0.4) | 86 | 1.1 | (0.2) |
| 47 | 9.1 | (0.3) | | | |
| 48 | 10.5 | (0.3) | | | |
| 49 | 10.7 | (0.5) | | | |
| 50 | 11.9 | (0.6) | | | |
| 51 | 13.3 | (0.5) | | | |
| 52 | 13.4 | (0.7) | | | |
| 53 | 15.2 | (0.6) | | | |
| 54 | 16.4 | (0.5) | | | |
| 55 | 12.2 | (0.6) | | | |
| 56 | 0.0 | (0.0) | | | |
| 57 | 12.1 | (0.5) | | | |
| 58 | 16.0 | (0.9) | | | |
| 59 | 13.7 | (0.7) | | | |
| 60 | 11.6 | (0.5) | | | |
| 61 | 10.5 | (0.4) | | | |

THE TOTAL RELAXATION RATE OUT OF J= 56: K(TOT)= 3.8368E-10

Table A-1. Rate Coefficeints for ICl + He Collisions (Continued)

| ICl + He ($J_i$ = 70, $v_i'$=1) | | | ICl + He ($J_i$ = 70, $v_i'$=1) | | |
|---|---|---|---|---|---|
| | ($10^{-12}$ cm$^3$ molecule$^{-1}$ s$^{-1}$) | | | ($10^{-12}$ cm$^3$ molecule$^{-1}$ s$^{-1}$) | |
| $J_f$ | $k(J_i,J_f)$ | $\sigma$ | $J_f$ | $k(J_i,J_f)$ | $\sigma$ |
| 31 | 1.9 | 0.9 | 71 | 13.4 | 0.8 |
| 32 | 2.4 | 1.1 | 72 | 16.8 | 1.1 |
| 33 | 1.7 | 0.5 | 73 | 13.4 | 0.5 |
| 34 | 2.3 | 0.8 | 74 | 11.4 | 1.4 |
| 35 | 2.4 | 0.8 | 75 | 10.2 | 0.7 |
| 36 | 0.9 | 1.0 | 76 | 10.5 | 1.7 |
| 37 | 3.0 | 1.1 | 77 | 7.8 | 0.4 |
| 38 | 2.4 | 0.5 | 78 | 8.5 | 0.5 |
| 39 | 2.8 | 0.7 | 79 | 6.1 | 1.2 |
| 40 | 0.8 | 1.0 | 80 | 4.5 | 0.6 |
| 41 | 2.7 | 0.8 | 81 | 3.1 | 0.8 |
| 42 | 3.7 | 0.5 | 82 | 7.9 | 1.0 |
| 43 | 3.1 | 0.6 | 83 | 5.9 | 1.0 |
| 44 | 3.4 | 1.1 | 84 | 6.1 | 0.8 |
| 45 | 4.0 | 0.6 | 85 | 3.8 | 0.8 |
| 46 | 4.2 | 0.6 | 86 | 2.1 | 0.9 |
| 47 | 3.6 | 0.8 | 87 | 2.0 | 0.4 |
| 48 | 5.1 | 1.1 | 88 | 1.4 | 0.6 |
| 49 | 4.6 | 1.1 | 89 | 1.3 | 0.5 |
| 50 | 4.8 | 0.8 | 90 | 0.8 | 0.3 |
| 51 | 4.6 | 0.6 | | | |
| 52 | 6.2 | 0.7 | | | |
| 53 | 5.9 | 0.6 | | | |
| 54 | 5.1 | 0.8 | | | |
| 55 | 5.1 | 0.8 | | | |
| 56 | 5.9 | 0.4 | | | |
| 57 | 5.0 | 0.5 | | | |
| 58 | 6.9 | 0.6 | | | |
| 59 | 7.3 | 0.4 | | | |
| 60 | 8.6 | 0.6 | | | |
| 61 | 10.1 | 1.1 | | | |
| 62 | 6.4 | 1.1 | | | |
| 63 | 11.3 | 1.1 | | | |
| 64 | 9.4 | 0.7 | | | |
| 65 | 12.5 | 1.2 | | | |
| 66 | 10.3 | 0.8 | | | |
| 67 | 13.5 | 1.1 | | | |
| 68 | 14.6 | 1.2 | | | |
| 69 | 13.4 | 1.0 | | | |
| 70 | 0.0 | 0.0 | | | |

Table A-2 Rate Coefficients for ICl + Kr Collisions

| ICl + Kr ($J_i$ = 26, $v_i$ = 1) | | | ICl + Kr ($J_i$ = 26, $v_i$ = 1) | | |
|---|---|---|---|---|---|
| | ($10^{-12}$ cm$^3$ molecule$^{-1}$ s$^{-1}$) | | | ($10^{-12}$ cm$^3$ molecule$^{-1}$ s$^{-1}$) | |
| $J_f$ | $k(J_i,J_f)$ | $\sigma$ | $J_f$ | $k(J_i,J_f)$ | $\sigma$ |
| 20 | 10.9 | 0.8 | 61 | 2.6 | 0.1 |
| 21 | 9.9 | 0.5 | 62 | 2.7 | 0.1 |
| 22 | 10.9 | 0.6 | 63 | 2.4 | 0.1 |
| 23 | 9.8 | 0.6 | 64 | 2.2 | 0.1 |
| 24 | 10.5 | 1.2 | 65 | 2.1 | 0.1 |
| 25 | 11.4 | 1.0 | 66 | 2.1 | 0.1 |
| 26 | 0.0 | 0.0 | | | |
| 27 | 12.0 | 1.9 | | | |
| 28 | 14.0 | 0.5 | | | |
| 29 | 10.1 | 0.3 | | | |
| 30 | 10.8 | 0.4 | | | |
| 31 | 10.8 | 0.4 | | | |
| 32 | 10.3 | 0.5 | | | |
| 33 | 9.4 | 0.3 | | | |
| 34 | 8.9 | 0.3 | | | |
| 35 | 8.4 | 0.3 | | | |
| 36 | 7.9 | 0.6 | | | |
| 37 | 6.9 | 0.2 | | | |
| 38 | 7.4 | 0.3 | | | |
| 39 | 7.1 | 0.2 | | | |
| 40 | 6.4 | 0.2 | | | |
| 41 | 6.0 | 0.2 | | | |
| 42 | 6.2 | 0.1 | | | |
| 43 | 6.0 | 0.1 | | | |
| 44 | 5.9 | 0.1 | | | |
| 45 | 6.0 | 0.3 | | | |
| 46 | 5.6 | 0.1 | | | |
| 47 | 5.3 | 0.1 | | | |
| 48 | 4.9 | 0.1 | | | |
| 49 | 5.0 | 0.1 | | | |
| 50 | 4.8 | 0.1 | | | |
| 51 | 4.5 | 0.0 | | | |
| 52 | 4.2 | 0.0 | | | |
| 53 | 4.0 | 0.0 | | | |
| 54 | 3.9 | 0.1 | | | |
| 55 | 3.6 | 0.1 | | | |
| 56 | 3.5 | 0.1 | | | |
| 57 | 3.5 | 0.1 | | | |
| 58 | 3.3 | 0.1 | | | |
| 59 | 3.1 | 0.1 | | | |
| 60 | 2.7 | 0.1 | | | |

Table A-2 Rate Coefficients for ICl + Kr Collisions

| ICl + Kr ($J_i$ = 34, $v_i'$=1) | | | ICl + Kr ($J_i$ = 34, $v_i'$=1) | | |
|---|---|---|---|---|---|
| | ($10^{-12}$ cm$^3$ molecule$^{-1}$ s$^{-1}$) | | | ($10^{-12}$ cm$^3$ molecule$^{-1}$ s$^{-1}$) | |
| $J_f$ | $k(J_i,J_f)$ | $\sigma$ | $J_f$ | $k(J_i,J_f)$ | $\sigma$ |
| 27 | 16.1 | 0.5 | 68 | 2.0 | 0.1 |
| 28 | 11.1 | 0.3 | 69 | 2.0 | 0.1 |
| 29 | 8.7 | 0.3 | 70 | 1.8 | 0.1 |
| 30 | 9.1 | 0.3 | 71 | 1.7 | 0.1 |
| 31 | 8.6 | 0.5 | 72 | 1.5 | 0.1 |
| 32 | 7.3 | 0.7 | 73 | 1.3 | 0.1 |
| 33 | 3.3 | 1.2 | 74 | 1.2 | 0.1 |
| 34 | 0.0 | 0.0 | | | |
| 35 | 6.6 | 0.5 | | | |
| 36 | 3.4 | 0.3 | | | |
| 37 | 7.2 | 0.4 | | | |
| 38 | 8.3 | 0.4 | | | |
| 39 | 7.6 | 0.3 | | | |
| 40 | 7.7 | 0.2 | | | |
| 41 | 7.5 | 0.3 | | | |
| 42 | 7.3 | 0.2 | | | |
| 43 | 7.1 | 0.2 | | | |
| 44 | 7.0 | 0.2 | | | |
| 45 | 8.0 | 0.2 | | | |
| 46 | 6.3 | 0.2 | | | |
| 47 | 5.8 | 0.1 | | | |
| 48 | 5.8 | 0.2 | | | |
| 49 | 5.4 | 0.2 | | | |
| 50 | 5.4 | 0.1 | | | |
| 51 | 5.1 | 0.1 | | | |
| 52 | 4.7 | 0.1 | | | |
| 53 | 4.4 | 0.1 | | | |
| 54 | 4.0 | 0.1 | | | |
| 55 | 4.1 | 0.1 | | | |
| 56 | 3.9 | 0.1 | | | |
| 57 | 3.9 | 0.1 | | | |
| 58 | 3.9 | 0.1 | | | |
| 59 | 3.8 | 0.1 | | | |
| 60 | 3.3 | 0.1 | | | |
| 61 | 3.0 | 0.1 | | | |
| 62 | 3.0 | 0.1 | | | |
| 63 | 2.6 | 0.1 | | | |
| 64 | 2.5 | 0.1 | | | |
| 65 | 2.4 | 0.1 | | | |
| 66 | 2.3 | 0.1 | | | |
| 67 | 2.1 | 0.1 | | | |

Table A-2 Rate Coefficients for ICl + Kr Collisions (Continued)

| ICl + Kr ($J_i$ = 56, $v_i'$=1) | | | ICl + Kr ($J_i$ = 26, $v_i'$=1) | | |
|---|---|---|---|---|---|
| | ($10^{-12}$ cm$^3$ molecule$^{-1}$ s$^{-1}$) | | | ($10^{-12}$ cm$^3$ molecule$^{-1}$ s$^{-1}$) | |
| $J_f$ | $k(J_i,J_f)$ | $\sigma$ | $J_f$ | $k(J_i,J_f)$ | $\sigma$ |
| 17 | 6.4 | 0.6 | 56 | 0.0 | 0.0 |
| 18 | 4.9 | 0.5 | 57 | 6.5 | 0.4 |
| 19 | 5.6 | 0.4 | 58 | 7.6 | 0.5 |
| 20 | 6.6 | 0.5 | 59 | 6.8 | 0.3 |
| 21 | 5.8 | 0.3 | 60 | 6.2 | 0.3 |
| 22 | 6.5 | 0.3 | 61 | 6.1 | 0.2 |
| 23 | 5.4 | 0.5 | 62 | 5.2 | 0.2 |
| 24 | 4.9 | 0.4 | 63 | 4.6 | 0.2 |
| 25 | 4.8 | 0.4 | 64 | 4.9 | 0.1 |
| 26 | 3.7 | 0.5 | 65 | 4.5 | 0.2 |
| 27 | 4.6 | 0.4 | 66 | 4.3 | 0.3 |
| 28 | 4.5 | 0.4 | 67 | 3.9 | 0.3 |
| 29 | 4.0 | 0.3 | 68 | 3.9 | 0.2 |
| 30 | 5.0 | 0.3 | 69 | 3.4 | 0.1 |
| 31 | 5.5 | 0.4 | 70 | 3.3 | 0.3 |
| 32 | 6.2 | 0.3 | 71 | 2.7 | 0.1 |
| 33 | 6.3 | 0.2 | 72 | 2.9 | 0.1 |
| 34 | 7.4 | 0.4 | 73 | 2.2 | 0.1 |
| 35 | 7.6 | 0.4 | 74 | 2.1 | 0.1 |
| 36 | 6.9 | 0.3 | 75 | 1.7 | 0.2 |
| 37 | 7.0 | 0.3 | 76 | 1.7 | 0.2 |
| 38 | 6.8 | 0.3 | 77 | 1.5 | 0.2 |
| 39 | 6.6 | 0.5 | 78 | 1.5 | 0.1 |
| 40 | 6.4 | 0.3 | 79 | 1.4 | 0.1 |
| 41 | 6.0 | 0.2 | 80 | 1.5 | 0.1 |
| 42 | 6.2 | 0.4 | 81 | 1.3 | 0.2 |
| 43 | 5.5 | 0.2 | 82 | 1.2 | 0.1 |
| 44 | 5.9 | 0.4 | 83 | 1.3 | 0.1 |
| 45 | 6.5 | 0.2 | 84 | 1.2 | 0.1 |
| 46 | 6.5 | 0.3 | 85 | 1.3 | 0.1 |
| 47 | 6.7 | 0.2 | 86 | 0.8 | 0.1 |
| 48 | 7.1 | 0.2 | | | |
| 49 | 6.9 | 0.4 | | | |
| 50 | 7.7 | 0.2 | | | |
| 51 | 8.1 | 0.4 | | | |
| 52 | 8.2 | 0.4 | | | |
| 53 | 8.3 | 0.3 | | | |
| 54 | 8.3 | 0.4 | | | |
| 55 | 6.9 | 0.6 | | | |

Table A-2 Rate Coefficients for ICl + Kr Collisions (Continued)

| ICl + Kr ($J_i$ = 61, $v_i'$=1) | | | ICl + Kr ($J_i$ = 61, $v_i'$=1) | | |
|---|---|---|---|---|---|
| | ($10^{-12}$ cm$^3$ molecule$^{-1}$ s$^{-1}$) | | | ($10^{-12}$ cm$^3$ molecule$^{-1}$ s$^{-1}$) | |
| $J_f$ | $k(J_i,J_f)$ | $\sigma$ | $J_f$ | $k(J_i,J_f)$ | $\sigma$ |
| 22 | 4.5 | 0.6 | 60 | 7.3 | 1.3 |
| 23 | 3.6 | 0.3 | 61 | 0.0 | 0.0 |
| 24 | 5.4 | 0.4 | 62 | 7.6 | 1.0 |
| 25 | 8.9 | 0.8 | 63 | 6.9 | 0.6 |
| 26 | 6.9 | 0.7 | 64 | 6.2 | 0.6 |
| 27 | 5.5 | 0.5 | 65 | 6.0 | 0.4 |
| 28 | 5.9 | 0.6 | 66 | 5.3 | 0.4 |
| 29 | 5.9 | 0.4 | 67 | 5.0 | 0.4 |
| 30 | 6.3 | 0.2 | 68 | 4.9 | 0.3 |
| 31 | 6.6 | 0.5 | 69 | 4.6 | 0.3 |
| 32 | 6.9 | 0.6 | 70 | 4.9 | 0.5 |
| 33 | 5.0 | 0.3 | 71 | 4.0 | 0.3 |
| 34 | 3.6 | 0.2 | 72 | 3.2 | 0.2 |
| 35 | 5.9 | 0.5 | 73 | 3.7 | 0.2 |
| 36 | 5.9 | 0.4 | 74 | 3.2 | 0.3 |
| 37 | 5.8 | 0.5 | 75 | 2.9 | 0.3 |
| 38 | 5.9 | 0.4 | 76 | 2.6 | 0.3 |
| 39 | 5.2 | 0.4 | 77 | 2.6 | 0.2 |
| 40 | 5.7 | 0.3 | 78 | 2.4 | 0.2 |
| 41 | 6.1 | 0.4 | 79 | 2.4 | 0.3 |
| 42 | 6.8 | 0.5 | 80 | 2.2 | 0.1 |
| 43 | 6.3 | 0.3 | 81 | 2.0 | 0.1 |
| 44 | 6.4 | 0.3 | 82 | 1.8 | 0.1 |
| 45 | 6.5 | 0.5 | 83 | 1.5 | 0.1 |
| 46 | 6.5 | 0.2 | 84 | 1.7 | 0.2 |
| 47 | 6.6 | 0.5 | 85 | 1.5 | 0.1 |
| 48 | 7.0 | 0.4 | 86 | 1.5 | 0.2 |
| 49 | 6.4 | 0.4 | 87 | 1.2 | 0.1 |
| 50 | 6.4 | 0.2 | 88 | 0.8 | 0.1 |
| 51 | 7.0 | 0.3 | 89 | 0.6 | 0.0 |
| 52 | 6.7 | 0.3 | 90 | 0.7 | 0.1 |
| 53 | 6.8 | 0.4 | 91 | 0.5 | 0.1 |
| 54 | 6.9 | 0.4 | | | |
| 55 | 7.1 | 0.5 | | | |
| 56 | 7.2 | 0.5 | | | |
| 57 | 7.7 | 0.6 | | | |
| 58 | 8.5 | 0.7 | | | |
| 59 | 8.7 | 0.9 | | | |

Table A-3. Rate Coefficients for ICl + Xe Collisions

| ICl + Xe ($J_i$ = 26, $v_i$ = 1) | | | ICl + Xe ($J_i$ = 26, $v_i$ = 1) | | |
|---|---|---|---|---|---|
| | ($10^{-12}$ cm$^3$ molecule$^{-1}$ s$^{-1}$) | | | ($10^{-12}$ cm$^3$ molecule$^{-1}$ s$^{-1}$) | |
| $J_f$ | $k(J_i,J_f)$ | $\sigma$ | $J_f$ | $k(J_i,J_f)$ | $\sigma$ |
| 18 | 7.6 | 1.4 | 55 | 3.4 | 0.1 |
| 19 | 8.2 | 1.0 | 56 | 3.5 | 0.2 |
| 20 | 8.9 | 0.6 | 57 | 3.4 | 0.1 |
| 21 | 8.8 | 0.5 | 58 | 3.1 | 0.1 |
| 22 | 9.4 | 0.6 | 59 | 3.0 | 0.1 |
| 23 | 9.6 | 0.4 | 60 | 2.7 | 0.1 |
| 24 | 10.8 | 0.5 | 61 | 2.5 | 0.1 |
| 25 | 11.3 | 1.3 | 62 | 2.3 | 0.1 |
| 26 | 0.0 | 0.0 | 63 | 2.3 | 0.1 |
| 27 | 10.7 | 0.8 | 64 | 2.2 | 0.1 |
| 28 | 9.6 | 0.5 | 65 | 1.9 | 0.1 |
| 29 | 10.3 | 0.3 | 66 | 1.9 | 0.1 |
| 30 | 9.6 | 0.3 | | | |
| 31 | 9.3 | 0.3 | | | |
| 32 | 9.0 | 0.3 | | | |
| 33 | 8.4 | 0.1 | | | |
| 34 | 8.1 | 0.1 | | | |
| 35 | 7.6 | 0.1 | | | |
| 36 | 7.2 | 0.1 | | | |
| 37 | 7.0 | 0.3 | | | |
| 38 | 6.3 | 0.2 | | | |
| 39 | 6.8 | 0.2 | | | |
| 40 | 6.3 | 0.2 | | | |
| 41 | 6.4 | 0.1 | | | |
| 42 | 6.1 | 0.1 | | | |
| 43 | 5.9 | 0.1 | | | |
| 44 | 6.0 | 0.3 | | | |
| 45 | 5.3 | 0.3 | | | |
| 46 | 5.3 | 0.2 | | | |
| 47 | 4.9 | 0.1 | | | |
| 48 | 4.7 | 0.1 | | | |
| 49 | 4.5 | 0.1 | | | |
| 50 | 4.3 | 0.1 | | | |
| 51 | 4.2 | 0.1 | | | |
| 52 | 4.0 | 0.1 | | | |
| 53 | 3.9 | 0.1 | | | |
| 54 | 3.5 | 0.1 | | | |

Table A-3. Rate Coefficients for ICl + Xe Collisions (Continued)

| ICl + Xe ($J_i$ = 34, $v_i$=1) | | | ICl + Xe ($J_i$ = 26, $v_i$=1) | | |
|---|---|---|---|---|---|
| | ($10^{-12}$ cm$^3$ molecule$^{-1}$ s$^{-1}$) | | | ($10^{-12}$ cm$^3$ molecule$^{-1}$ s$^{-1}$) | |
| $J_f$ | $k(J_i,J_f)$ | $\sigma$ | $J_f$ | $k(J_i,J_f)$ | $\sigma$ |
| 27 | 14.7 | 0.4 | 65 | 2.3 | 0.1 |
| 28 | 11.8 | 0.4 | 66 | 2.2 | 0.1 |
| 29 | 9.3 | 0.4 | 67 | 2.0 | 0.1 |
| 30 | 9.2 | 0.3 | 68 | 1.9 | 0.1 |
| 31 | 9.3 | 0.3 | 69 | 1.7 | 0.1 |
| 32 | 8.6 | 0.3 | 70 | 1.7 | 0.1 |
| 33 | 7.7 | 0.9 | 71 | 1.5 | 0.1 |
| 34 | 0.0 | 0.0 | 72 | 1.5 | 0.1 |
| 35 | 11.7 | 0.5 | 73 | 1.2 | 0.1 |
| 36 | 4.8 | 0.3 | 74 | 1.0 | 0.1 |
| 37 | 7.0 | 0.2 | | | |
| 38 | 8.3 | 0.3 | | | |
| 39 | 7.7 | 0.3 | | | |
| 40 | 7.6 | 0.2 | | | |
| 41 | 7.5 | 0.4 | | | |
| 42 | 7.2 | 0.2 | | | |
| 43 | 7.1 | 0.2 | | | |
| 44 | 6.9 | 0.1 | | | |
| 45 | 7.8 | 0.2 | | | |
| 46 | 6.3 | 0.2 | | | |
| 47 | 5.5 | 0.1 | | | |
| 48 | 5.2 | 0.2 | | | |
| 49 | 5.2 | 0.1 | | | |
| 50 | 5.1 | 0.1 | | | |
| 51 | 4.9 | 0.1 | | | |
| 52 | 5.7 | 0.2 | | | |
| 53 | 4.2 | 0.3 | | | |
| 54 | 3.9 | 0.1 | | | |
| 55 | 4.0 | 0.1 | | | |
| 56 | 4.2 | 0.1 | | | |
| 57 | 4.0 | 0.2 | | | |
| 58 | 3.6 | 0.1 | | | |
| 59 | 3.2 | 0.2 | | | |
| 60 | 2.9 | 0.1 | | | |
| 61 | 2.9 | 0.1 | | | |
| 62 | 2.9 | 0.1 | | | |
| 63 | 2.7 | 0.1 | | | |
| 64 | 2.7 | 0.1 | | | |

Table A-3. Rate Coefficients for ICl + Xe Collisions (Continued)

| ICl + Xe ($J_i$ = 56, $v_i'$=1) | | | ICl + Xe ($J_i$ = 56, $v_i'$=1) | | |
|---|---|---|---|---|---|
| | ($10^{-12}$ cm$^3$ molecule$^{-1}$ s$^{-1}$) | | | ($10^{-12}$ cm$^3$ molecule$^{-1}$ s$^{-1}$) | |
| $J_f$ | $k(J_i,J_f)$ | $\sigma$ | $J_f$ | $k(J_i,J_f)$ | $\sigma$ |
| 17 | 7.7 | 0.4 | 56 | 0.0 | 0.0 |
| 18 | 9.3 | 0.7 | 57 | 3.8 | 0.5 |
| 19 | 9.3 | 0.7 | 58 | 6.4 | 0.4 |
| 20 | 9.4 | 0.7 | 59 | 6.7 | 0.2 |
| 21 | 9.3 | 0.6 | 60 | 7.3 | 0.2 |
| 22 | 11.2 | 0.7 | 61 | 7.2 | 0.2 |
| 23 | 8.0 | 0.4 | 62 | 6.6 | 0.3 |
| 24 | 6.4 | 0.5 | 63 | 6.6 | 0.3 |
| 25 | 6.3 | 0.6 | 64 | 6.2 | 0.2 |
| 26 | 6.4 | 0.4 | 65 | 5.7 | 0.2 |
| 27 | 6.1 | 0.5 | 66 | 5.3 | 0.3 |
| 28 | 6.7 | 0.4 | 67 | 5.4 | 0.2 |
| 29 | 8.3 | 0.5 | 68 | 4.7 | 0.2 |
| 30 | 6.7 | 0.4 | 69 | 4.2 | 0.3 |
| 31 | 7.9 | 0.5 | 70 | 4.0 | 0.3 |
| 32 | 10.0 | 0.5 | 71 | 3.6 | 0.2 |
| 33 | 11.4 | 0.6 | 72 | 3.3 | 0.1 |
| 34 | 10.6 | 0.4 | 73 | 3.6 | 0.2 |
| 35 | 11.6 | 0.4 | 74 | 2.7 | 0.2 |
| 36 | 11.7 | 0.4 | 75 | 2.6 | 0.2 |
| 37 | 10.8 | 0.4 | 76 | 2.6 | 0.2 |
| 38 | 11.0 | 0.2 | 77 | 2.4 | 0.2 |
| 39 | 11.2 | 0.4 | 78 | 2.6 | 0.2 |
| 40 | 10.2 | 0.3 | 79 | 1.9 | 0.1 |
| 41 | 9.1 | 0.4 | 80 | 2.0 | 0.1 |
| 42 | 8.7 | 0.2 | 81 | 1.7 | 0.1 |
| 43 | 8.5 | 0.4 | 82 | 1.7 | 0.1 |
| 44 | 9.3 | 0.3 | 83 | 1.6 | 0.2 |
| 45 | 9.6 | 0.3 | 84 | 1.2 | 0.2 |
| 46 | 8.9 | 0.4 | 85 | 1.2 | 0.2 |
| 47 | 9.4 | 0.2 | 86 | 1.0 | 0.2 |
| 48 | 9.6 | 0.1 | | | |
| 49 | 9.7 | 0.3 | | | |
| 50 | 9.8 | 0.2 | | | |
| 51 | 10.2 | 0.3 | | | |
| 52 | 9.9 | 0.3 | | | |
| 53 | 9.0 | 0.3 | | | |
| 54 | 7.3 | 0.3 | | | |
| 55 | 4.4 | 0.4 | | | |

Table A-3. Rate Coefficients for ICl + Xe Collisions (Continued)

| ICl + Xe ($J_i$ = 70, $v_i'$=1) | | | ICl + Xe ($J_i$ = 70, $v_i'$=1) | | |
|---|---|---|---|---|---|
| | ($10^{-12}$ cm$^3$ molecule$^{-1}$ s$^{-1}$) | | | ($10^{-12}$ cm$^3$ molecule$^{-1}$ s$^{-1}$) | |
| $J_f$ | $k(J_i,J_f)$ | $\sigma$ | $J_f$ | $k(J_i,J_f)$ | $\sigma$ |
| 31 | 6.9 | 0.8 | 68 | 6.1 | 0.8 |
| 32 | 7.9 | 0.6 | 69 | 4.2 | 0.7 |
| 33 | 7.8 | 0.8 | 70 | 0.0 | 0.0 |
| 34 | 11.1 | 1.0 | 71 | 5.0 | 0.5 |
| 35 | 8.7 | 1.0 | 72 | 6.3 | 0.4 |
| 36 | 8.9 | 0.4 | 73 | 7.1 | 0.4 |
| 37 | 9.9 | 0.4 | 74 | 6.0 | 0.4 |
| 38 | 9.8 | 0.5 | 75 | 5.1 | 0.5 |
| 39 | 8.8 | 0.7 | 76 | 6.0 | 0.4 |
| 40 | 8.6 | 0.7 | 77 | 4.5 | 0.3 |
| 41 | 8.0 | 0.4 | 78 | 5.7 | 0.5 |
| 42 | 6.9 | 0.3 | 79 | 3.0 | 0.5 |
| 43 | 7.4 | 0.5 | 80 | 4.6 | 0.3 |
| 44 | 8.3 | 0.5 | 81 | 3.1 | 0.3 |
| 45 | 8.8 | 0.4 | 82 | 2.6 | 0.6 |
| 46 | 6.9 | 0.5 | 83 | 1.7 | 0.3 |
| 47 | 8.1 | 0.4 | 84 | 2.6 | 0.4 |
| 48 | 7.4 | 0.4 | 85 | 2.1 | 0.3 |
| 49 | 7.2 | 0.5 | 86 | 1.5 | 0.2 |
| 50 | 9.0 | 0.5 | 87 | 2.0 | 0.3 |
| 51 | 9.6 | 0.4 | 88 | 0.7 | 0.4 |
| 52 | 9.6 | 0.7 | 89 | 1.4 | 0.5 |
| 53 | 8.4 | 0.5 | 90 | 0.4 | 0.1 |
| 54 | 8.5 | 0.5 | | | |
| 55 | 7.7 | 0.3 | | | |
| 56 | 8.1 | 0.5 | | | |
| 57 | 10.2 | 0.5 | | | |
| 58 | 8.2 | 0.4 | | | |
| 59 | 7.2 | 0.3 | | | |
| 60 | 8.0 | 0.7 | | | |
| 61 | 7.9 | 0.3 | | | |
| 62 | 6.5 | 0.8 | | | |
| 63 | 6.7 | 0.3 | | | |
| 64 | 6.3 | 0.4 | | | |
| 65 | 6.7 | 0.6 | | | |
| 66 | 7.3 | 0.6 | | | |
| 67 | 7.9 | 0.7 | | | |

Table A-4. Rate Coefficients for ICl + ICl Collisions

| ICl + ICl ($J_i$ = 35, $v_i'$=1) | | | ICl + ICl ($J_i$ = 35, $v_i'$=1) | | |
|---|---|---|---|---|---|
| | ($10^{-12}$ cm$^3$ molecule$^{-1}$ s$^{-1}$) | | | ($10^{-12}$ cm$^3$ molecule$^{-1}$ s$^{-1}$) | |
| $J_f$ | $k(J_i,J_f)$ | $\sigma$ | $J_f$ | $k(J_i,J_f)$ | $\sigma$ |
| 27 | 14.7 | 3.4 | 67 | 3.8 | 0.3 |
| 28 | 20.3 | 0.9 | 68 | 3.8 | 0.3 |
| 29 | 23.7 | 1.3 | 69 | 3.1 | 0.3 |
| 30 | 23.8 | 1.0 | 70 | 3.0 | 0.2 |
| 31 | 27.4 | 1.7 | 71 | 2.5 | 0.1 |
| 32 | 34.1 | 1.2 | 72 | 2.2 | 0.2 |
| 33 | 45.9 | 1.2 | 73 | 1.4 | 0.3 |
| 34 | 70.7 | 2.5 | 74 | 1.2 | 0.2 |
| 35 | 0.0 | 0.0 | 75 | 1.2 | 0.2 |
| 36 | 71.1 | 2.7 | 76 | 1.5 | 0.2 |
| 37 | 37.7 | 1.0 | 77 | 1.4 | 0.1 |
| 38 | 28.5 | 0.8 | 78 | 1.4 | 0.2 |
| 39 | 20.8 | 0.9 | 79 | 1.3 | 0.1 |
| 40 | 17.5 | 0.9 | 80 | 1.4 | 0.2 |
| 41 | 15.2 | 0.9 | 81 | 1.0 | 0.1 |
| 42 | 10.5 | 1.0 | 82 | 1.0 | 0.2 |
| 43 | 12.9 | 0.5 | 83 | 1.3 | 0.2 |
| 44 | 12.3 | 0.5 | 84 | 1.1 | 0.2 |
| 45 | 11.9 | 0.5 | | | |
| 46 | 11.3 | 0.4 | | | |
| 47 | 12.0 | 0.5 | | | |
| 48 | 9.2 | 0.5 | | | |
| 49 | 8.3 | 0.6 | | | |
| 50 | 10.0 | 0.4 | | | |
| 51 | 10.2 | 0.4 | | | |
| 52 | 8.3 | 0.2 | | | |
| 53 | 7.8 | 0.2 | | | |
| 54 | 7.5 | 0.2 | | | |
| 55 | 7.0 | 0.2 | | | |
| 56 | 6.1 | 0.2 | | | |
| 57 | 6.2 | 0.4 | | | |
| 58 | 5.2 | 0.4 | | | |
| 59 | 3.1 | 0.6 | | | |
| 60 | 4.6 | 0.4 | | | |
| 61 | 4.8 | 0.4 | | | |
| 62 | 5.0 | 0.3 | | | |
| 63 | 4.5 | 0.2 | | | |
| 64 | 3.5 | 0.4 | | | |
| 65 | 3.9 | 0.3 | | | |
| 66 | 3.8 | 0.2 | | | |

Table A-4. Rate Coefficients for ICl + ICl Collisions (Continued)

| ICl + ICl ($J_i$ = 57, $v_i'$ = 1) | | | ICl + ICl ($J_i$ = 57, $v_i'$ = 1) | | |
|---|---|---|---|---|---|
| | ($10^{-12}$ cm$^3$ molecule$^{-1}$ s$^{-1}$) | | | ($10^{-12}$ cm$^3$ molecule$^{-1}$ s$^{-1}$) | |
| $J_f$ | $k(J_i,J_f)$ | $\sigma$ | $J_f$ | $k(J_i,J_f)$ | $\sigma$ |
| 11 | 6.9 | 1.0 | 54 | 31.8 | 0.7 |
| 12 | 8.0 | 1.3 | 55 | 39.5 | 1.3 |
| 13 | 4.8 | 1.0 | 56 | 61.7 | 2.6 |
| 14 | 5.3 | 1.6 | 57 | 0.0 | 0.0 |
| 15 | 6.5 | 1.1 | 58 | 64.2 | 2.5 |
| 16 | 6.5 | 0.7 | 59 | 40.2 | 1.4 |
| 17 | 10.2 | 0.8 | 60 | 28.1 | 1.0 |
| 18 | 11.9 | 0.9 | 61 | 21.5 | 0.8 |
| 19 | 7.2 | 0.7 | 62 | 19.2 | 0.8 |
| 20 | 4.6 | 0.6 | 63 | 15.5 | 0.4 |
| 21 | 5.0 | 0.9 | 64 | 15.5 | 0.5 |
| 22 | 8.1 | 0.7 | 65 | 13.9 | 0.5 |
| 23 | 10.1 | 0.6 | 66 | 12.2 | 0.5 |
| 24 | 9.0 | 0.7 | 67 | 10.0 | 1.1 |
| 25 | 7.7 | 0.4 | 68 | 8.4 | 0.5 |
| 26 | 6.6 | 0.5 | 69 | 8.6 | 0.4 |
| 27 | 8.2 | 0.4 | 70 | 7.5 | 0.4 |
| 28 | 12.0 | 0.5 | 71 | 7.0 | 0.4 |
| 29 | 14.1 | 0.4 | 72 | 6.3 | 0.4 |
| 30 | 13.9 | 0.7 | 73 | 5.6 | 0.3 |
| 31 | 9.8 | 0.8 | 74 | 5.2 | 0.3 |
| 32 | 10.4 | 0.8 | 75 | 4.5 | 0.4 |
| 33 | 12.3 | 0.6 | 76 | 3.8 | 0.4 |
| 34 | 13.7 | 0.6 | 77 | 3.4 | 0.5 |
| 35 | 14.8 | 0.6 | 78 | 3.4 | 0.4 |
| 36 | 12.6 | 0.6 | 79 | 2.8 | 0.4 |
| 37 | 10.6 | 0.6 | 80 | 3.3 | 0.2 |
| 38 | 12.9 | 0.4 | 81 | 2.9 | 0.2 |
| 39 | 12.8 | 0.3 | 82 | 2.6 | 0.3 |
| 40 | 12.8 | 0.3 | 83 | 1.9 | 0.3 |
| 41 | 12.8 | 0.3 | 84 | 2.1 | 0.3 |
| 42 | 12.4 | 0.7 | 85 | 2.3 | 0.3 |
| 43 | 11.5 | 0.4 | 86 | 2.3 | 0.4 |
| 44 | 12.4 | 0.7 | 87 | 2.1 | 0.3 |
| 45 | 14.5 | 0.6 | 88 | 0.6 | 0.2 |
| 46 | 16.0 | 0.7 | 89 | 0.9 | 0.1 |
| 47 | 16.1 | 0.5 | 90 | 0.8 | 0.2 |
| 48 | 17.1 | 0.6 | 91 | 0.6 | 0.1 |
| 49 | 18.0 | 0.6 | 92 | 1.2 | 0.3 |
| 50 | 16.8 | 0.9 | 93 | 2.6 | 0.4 |
| 51 | 19.6 | 0.9 | 94 | 2.1 | 0.3 |
| 52 | 23.1 | 0.8 | 95 | 1.9 | 0.4 |
| 53 | 26.7 | 0.7 | | | |

Table A-4. Rate Coefficients for ICl + ICl Collisions (Continued)

| ICl + ICl ($J_i$ = 61, $v_i'$=1) | | | ICl + ICl ($J_i$ = 61, $v_i'$=1) | | |
|---|---|---|---|---|---|
| | ($10^{-12}$ cm$^3$ molecule$^{-1}$ s$^{-1}$) | | | ($10^{-12}$ cm$^3$ molecule$^{-1}$ s$^{-1}$) | |
| $J_f$ | $k(J_i,J_f)$ | $\sigma$ | $J_f$ | $k(J_i,J_f)$ | $\sigma$ |
| 18 | 7.8 | 1.5 | 59 | 44.0 | 1.4 |
| 19 | 6.9 | 1.0 | 60 | 60.3 | 1.4 |
| 20 | 7.4 | 1.4 | 61 | 0.0 | 0.0 |
| 21 | 6.6 | 1.0 | 62 | 53.1 | 2.0 |
| 22 | 4.3 | 1.0 | 63 | 37.3 | 1.0 |
| 23 | 6.7 | 0.6 | 64 | 28.9 | 2.3 |
| 24 | 9.5 | 1.0 | 65 | 21.4 | 0.8 |
| 25 | 14.6 | 1.0 | 66 | 17.1 | 1.1 |
| 26 | 11.6 | 1.2 | 67 | 16.1 | 1.9 |
| 27 | 9.1 | 1.7 | 68 | 15.9 | 1.0 |
| 28 | 9.9 | 1.9 | 69 | 13.7 | 0.9 |
| 29 | 10.6 | 0.7 | 70 | 14.2 | 1.8 |
| 30 | 13.1 | 1.1 | 71 | 11.3 | 0.9 |
| 31 | 14.2 | 1.4 | 72 | 10.0 | 0.7 |
| 32 | 12.6 | 1.2 | 73 | 8.2 | 0.4 |
| 33 | 9.5 | 1.2 | 74 | 6.5 | 0.8 |
| 34 | 8.5 | 0.8 | 75 | 6.7 | 0.5 |
| 35 | 12.1 | 1.1 | 76 | 6.4 | 0.4 |
| 36 | 11.4 | 1.0 | 77 | 5.9 | 0.4 |
| 37 | 10.5 | 1.2 | 78 | 5.2 | 0.4 |
| 38 | 10.7 | 0.9 | 79 | 4.6 | 0.4 |
| 39 | 10.6 | 0.7 | 80 | 4.5 | 0.5 |
| 40 | 8.6 | 0.5 | 81 | 4.8 | 0.4 |
| 41 | 11.8 | 0.8 | 82 | 4.0 | 0.5 |
| 42 | 14.3 | 1.0 | 83 | 3.9 | 0.4 |
| 43 | 12.1 | 0.6 | 84 | 3.1 | 0.5 |
| 44 | 12.7 | 0.6 | 85 | 4.5 | 0.5 |
| 45 | 12.1 | 1.3 | 86 | 4.5 | 0.4 |
| 46 | 14.0 | 0.7 | 87 | 3.9 | 0.3 |
| 47 | 13.8 | 0.8 | 88 | 1.7 | 0.4 |
| 48 | 15.0 | 0.8 | 89 | 1.7 | 0.2 |
| 49 | 14.7 | 1.0 | 90 | 1.4 | 0.2 |
| 50 | 13.5 | 0.9 | 91 | 0.9 | 0.4 |
| 51 | 12.4 | 0.9 | 92 | 2.6 | 0.4 |
| 52 | 15.5 | 0.7 | 93 | 4.7 | 0.5 |
| 53 | 17.5 | 0.6 | 94 | 4.6 | 0.6 |
| 54 | 17.5 | 0.9 | 95 | 4.8 | 0.7 |
| 55 | 19.2 | 0.8 | | | |
| 56 | 21.9 | 0.6 | | | |
| 57 | 25.3 | 0.7 | | | |
| 58 | 32.2 | 1.1 | | | |